

INTERFACIAL PARTITIONING DURING SOLIDIFICATION

by

JAMES C. BAKER

B.S. Michigan State University (1965)

M.S. Michigan State University (1966)

Submitted in Partial Fulfillment of the

Requirements for the Degree of

DOCTOR OF PHILOSOPHY

at the

MASSACHUSETTS INSTITUTE OF TECHNOLOGY

June, 1970

Signature of Author

Department of Metallurgy
May 14, 1970

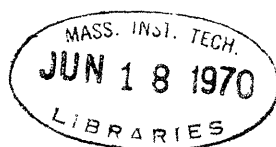
Certified by

Thesis Supervisor

Accepted by

Chairman, Departmental
Committee on
Graduate Students

Archives



INTERFACIAL PARTITIONING DURING SOLIDIFICATION

By

James C. Baker

Submitted to the Department of Metallurgy and Materials Science on May 14, 1970, in partial fulfillment of the requirement for the degree of Doctor of Philosophy.

ABSTRACT

It has been demonstrated experimentally that departures from local equilibrium at the interface do occur during rapid solidification of zinc-cadmium alloys. The resulting solid compositions are larger than the equilibrium solid compositions at any temperature, including metastable equilibrium compositions below the eutectic. This implies the solute chemical potential increases during the freezing process. Non-equilibrium alloy solidification theories of Jackson, Borisov, and Baralis cannot predict an increase in solute chemical potential, and therefore are invalid.

There is a group of theories that do predict an increase in chemical potential during freezing. This set of theories as well as the above set can both be derived from irreversible thermodynamics. The two types of theories can best be understood in the common framework of irreversible thermodynamics. Within this common framework contradictory predictions can be made from theories starting with identical assumptions. Therefore, the validity of both groups of theories is in doubt, and irreversible thermodynamics as currently applied is untrustworthy.

A kinetic theory is developed which indicates that if solute atoms are adsorbed on the liquid-solid interface then their chemical potential increases during the solidification process, even at low interface velocities.

Thesis Supervisor: John W. Cahn
Title: Professor of Physical Metallurgy

TABLE OF CONTENTS

<u>Section Number</u>		<u>Page Number</u>
	ABSTRACT	ii
	LIST OF ILLUSTRATIONS	iii
	ACKNOWLEDGEMENTS	vi
I	GENERAL INTRODUCTION	1
	1. Introduction	1
	2. Continuous Interface Motion in Pure Materials	2
	3. Equilibrium Segregation at Phase Boundaries	5
	4. Driving Force for Interface Motion in Binary Alloys	9
	5. Continuous Interface Motion in Binary Alloys	16
	6. Scope and Objective of Thesis	20
II	SOLUTE TRAPPING BY RAPID SOLIDIFICATION	31
	1. Introduction	31
	2. Experimental	33
	3. Discussion	34
	4. Appendix	40
III	THERMODYNAMIC ASPECTS OF SOLIDIFICATION PROBLEMS	50
	1. Introduction	50
	2. The Assumption of Local Equilibrium	54
	3. Steady-State Binary Solidification	56

<u>Section Number</u>		<u>Page Number</u>
IV	IRREVERSIBLE THERMODYNAMICS OF INTERFACE PROCESSES	65
	1. Introduction	65
	2. General Principles	65
	3. Solidification Theories	73
	A. Borisov Theory	73
	B. Jackson Theory	74
	C. Baralis Theory	75
	D. Aptekar-Kamenetskaya Theory	76
	E. Jindal-Tiller Theory	77
	4. Discussion of Theories	78
V	AN ALTERNATE APPROACH TO INTERFACE PARTITIONING DURING SOLIDIFICATION	81
	1. Introduction	81
	2. Diffusional Solution	81
	3. Graphical Representation	85
	4. Appendix	90
VI	SUMMARY AND GENERAL CONCLUSION	100
	1. Summary	100
	2. Suggestions for Future Work	101
	3. References	103
	4. Biographical Note	106

LIST OF ILLUSTRATIONS

<u>Figure Number</u>		<u>Page Number</u>
I-1	Graphical method for obtaining the chemical potentials from the molar free energy curve.	23
I-2	Graphical construction for obtaining the equilibrium chemical potentials and compositions from the free energy curves for a binary system.	24
I-3	Graphical method for obtaining the total free energy change of α when a mole of material of composition C is added to a large amount of α at composition C_α .	25
I-4	Graphical illustration of free energy ΔG per mole reacted for diffusionless reactions of composition C_0 from α to β .	26
I-5	When the ratios of the reacting components coincides with those of one of the phase, the general tangent-to-tangent rule for obtaining free energy changes reduces to a tangent-to-curve rule. Here $C_r = C_\beta$.	27
I-6	It is thermodynamically possible to form solid of any composition between $C_S(1)$ to $C_S(2)$ from liquid of composition C_0 .	28
I-7	The domain of all possible solid compositions that can form from various liquid compositions at a given temperature is enclosed within the curve OABEP. The curves OE and EP represent conditions of equal chemical potential for solute and solvent respectively. They are straight lines for dilute solutions. Their intersection E is the equilibrium condition. The line OB is for a diffusionless transformation, with B representing the T_0 condition.	29
I-8	Schematic free energy curves to illustrate the evolution of the curve OABEP of Figure I-7.	30

<u>Figure Number</u>		<u>Page Number</u>
II-1	Portion of phase diagram showing equilibrium composition of solid and liquid.	44
II-2	Portion of eutectic phase diagram illustrating equilibrium metastability of solid and liquid.	45
II-3	Zinc-cadmium retrograde phase diagram.	46
II-4	Plot of unit cell volume of zinc-rich solid at -196°C against weight per cent cadmium of initial liquid.	47
II-5	Electron micrograph of Zn-3.5 w/o Cd which was splat quenched to -196°C . 130,000X.	48
II-6	Electron micrograph of replica of Zn-3.5 w/o Cd which was cooled by the piston and anvil technique. 8,000X.	49
III-1	When there is a spinodal in the miscibility gap the stable-metastable phase diagram lines end when the solidus meets the spinodal. Further extensions of the metastable liquidus and solidus line are unstable and intersect at a point on the T_0 line.	62
III-2	The domain of possible liquid interface compositions for steady-state solidification of an alloy of composition C_0 at three different temperatures. At steady-state C_S equals C_0 . As indicated by the arrows upward fluctuations in solid composition reduce the solute content of the liquid and downward fluctuations increase it. Steady-state cannot be established by a system at point F in temperature region II. Local equilibrium cannot be maintained in region III.	63

<u>Figure Number</u>		<u>Page Number</u>
III-3	Liquidus, solidus and T_0 curves defining the three regions of temperature of Figure III-2.	64
IV-1	In the double primed set the free energy change per mole of solid formed ΔG_I is apportioned among a solidification reaction ΔG_S for which the driving force is $\Delta\mu$ averaged among the atoms in the liquid at the interface and a redistribution reaction in which the differences in $\Delta\mu$ act to bring about the composition difference $(C_L - C_S)$.	80
V-1	Graphical illustration of the inter-diffusion coefficient $D(x)$ and the solute interaction energy $E(x)$ as a function of distance x through the interface. The value of the solute interaction energy at the center of the boundary E_B will be allowed to vary from $E_B \ll E_L$ to $E_B \gg E_S$ in the analysis.	90
V-2	Partitioning at interface as a function of imposed growth rate.	91

ACKNOWLEDGEMENTS

The author wishes to express his sincere thanks to Professor John W. Cahn for his peerless guidance and continued encouragement throughout this investigation.

Helpful discussions with Professors K. C. Russell and M. C. Flemings are greatly appreciated. Thanks is also due to Dr. B. C. Giessen for his contribution of time and sputter cooling equipment.

Special thanks are due to Mrs. Janine Weins for her assistance in the electron microscopy portion of the study, and Dr. Ronald Heady for computer programming assistance.

The author is deeply indebted to his wife, Bonnie, for colossal patience and understanding throughout the course of the work.

The financial support of the National Science Foundation is gratefully appreciated.

Chapter I

GENERAL INTRODUCTION

I.1 Introduction

The purpose of this chapter is to give the reader the necessary background and a framework for understanding succeeding chapters. Consequently, a number of distinct concepts need mentioning, and for this reason the various sections of this chapter may appear to be somewhat unrelated.

An attempt will be made throughout the chapter to show that the same principles which apply to interface motion in solids, such as during recrystallization, can be used to describe and explain liquid-solid interface motion during solidification. The next section concerns itself with interface motion in pure materials during solidification and solid-solid transformations. A couple of theories of both types of transitions will be discussed. Section I.5 will later extend these suppositions to describe interface motion in binary systems. The key here is to account for the additional variable of composition.

Sections I.3 and I.4 pertain to aspects of interfaces which are vital prerequisites in understanding boundary motion in binary alloys. The last section gives a perspective view of the remainder of the thesis.

I.2 Continuous Interface Motion in Pure Materials

Before attempting to understand binary interface motion and the associated interface partitioning, a brief treatise of interface migration in pure materials will be given.

There are two general atomistic mechanisms of crystal growth from the melt. (a) The first is when the interface advances normal to itself. For this case the nature of the interface is usually thought of as being "rough" (1,2), or the driving force being sufficiently large (3). Wilson (4) in 1899 was the first to propose a kinetic theory to describe this type of freezing in pure materials. His prediction is of the form

$$V = -M\Delta G \quad (1.1)$$

where V is the growth rate, M is an interface mobility which is dependent on temperature, and ΔG is the change in the molar free energy (equal but opposite in sign to the driving free energy). This relationship is still popular today.

(b) The second mechanism is when the interface advances by lateral motion of steps or layers one or more interatomic distances in height. There is no normal advance of the interface, growth of an element of surface advances only when a layer sweeps by. A possible generation of such steps has been proposed by Frank (5) to occur

at screw dislocations. It was later shown by Hillig and Turnbull(6) that the growth rate by such a mechanism is

$$V \propto (\Delta G)^2 \quad (1.2)$$

Interface motion by steps is believed to occur when the liquid-solid interface is smooth(2), or when the driving force is sufficiently small(3). Regardless of the fact many materials are believed to solidify by this mechanism, the remainder of this thesis will be committed to a study of normal interface advancement. It will be called "continuous interface motion."

The first theories of continuous interface motion in solids were proposed by Turnbull(7) and Mott(8) for recrystallization. They derived rates of motion of high-angle grain boundaries by the use of absolute reaction-rate theory. Turnbull bases his theory on the assumption that the atoms traverse the interface individually. His final conclusion is

$$V = -e\lambda \left(\frac{kT}{h}\right) \left(\frac{\Delta G}{RT}\right) \exp\left(\frac{\Delta S_a}{R}\right) \exp\left(-\frac{Q_a}{RT}\right) \quad (1.3)$$

where e is the Napierian base, λ is the atomic jump distance, h is Planck's constant, N is Avogadro's number, ΔG is the molar free energy difference, ΔS_a is the entropy of activation, R is the universal gas constant, Q_a is the activation energy and T is the absolute temperature in Kelvin units.

If the structure of the interface is always assumed not to change then equation (1.3) can be written in the form of equation (1.1).

Mott's approach differs in that he assumes the interface transport process is one where groups of atoms of the parent grain melt and then solidify as a group onto the daughter grain. Mott's end result is of similar form to that of Turnbull's

$$V = -e\lambda \left(\frac{kT}{h}\right) \left(\frac{n\Delta G}{RT}\right) \exp\left(\frac{nL_m}{RT}\right) \exp\left(-\frac{nL_m}{RT}\right) \quad (1.4)$$

where n is the number of atoms in each group, T_m is the melting temperature and L_m is the latent heat of fusion.

Experimental boundary migration rates by Aust and Rutter(9), Rath and Hu(10), and Gordon and Vandermeer(11) show agreement with predictions of Turnbull's single-process theory, while Mott's group-process theory predicts a velocity of several orders of magnitude higher.

A similar approach to Turnbull's has been proposed specifically for liquid to solid transformations in pure materials by Jackson and Chalmers(12). This analysis is more detailed, though, because it considers geometric factors and the probability that an atom will be accommodated by one of the phases at the interface. The essential feature of the Turnbull theory that interface motion is the result of an individual atomic process is retained.

I.3 Equilibrium Segregation at Phase Boundaries

If theories similar to Turnbull's (7) are tested for materials without ultra-high purity large disagreements between theory and experiment result. The pre-exponential term is found to be much too small (11). Hence, impurities or solute atoms influence interface motion significantly. It is believed the solute retards the interface motion by segregating to the interface. For this reason it is of interest to digress temporarily to allow one to comprehend the interaction of a solute species with an interface. Before the role of solute on moving boundaries is considered, an attempt will be made to convey that which is known about segregation at stationary boundaries or interfaces.

A means of characterizing equilibrium segregation at boundaries will now be given. If one assumes the structure of the interface is different than the bulk phase or phases and hence the affinity for solute atoms is also unequal, then it is plausible to express the solute chemical potential of the system in terms of a solute interaction energy $E(x)$ in dilute solution as

$$\mu^B = kT \ln C(x) + E(x) + \text{constant} \quad (1.5)$$

The superscript B refers to the solute species. The distance x is in a direction normal to the interface. At equilibrium ($\mu = \text{constant}$), C and E will be constant in

the bulk phase. But if the boundary is considered to have a finite thickness, then C and E may vary with position in the boundary to maintain $\mu = \text{constant}$. In this thesis E_B will designate the value of E at the center of the boundary.

An understanding of the solute interaction energy E may be conceived by the following discussion. Consider the addition of a solute species to a pure material while keeping the addition small to minimize solute-solute interactions. If there is an attractive or repulsive force on the solute atoms in the vicinity of a boundary then this force can be perceived as minus the gradient of a potential energy. The solute interaction energy E is this potential energy. One would expect a higher concentration of solute where the interaction energy is lower. In equation (1.5) the first term may be thought of as the entropy contribution to μ and E the enthalpy contribution. For a given μ , such as at equilibrium, the smaller the solute interaction energy E the larger the composition C will be.

At equilibrium, if one sets the solute chemical potentials of the bulk phase α and of the boundary equal, then the ratio of solute compositions is given by

$$\frac{C_B(\text{eq})}{C_\alpha(\text{eq})} = \exp\left(\frac{E_\alpha - E_B}{kT}\right) \quad (1.6a)$$

The subscript B refers to the boundary. From this equation, it follows that if $E_{\alpha} > E_B$ then $C_B(\text{eq}) > C_{\alpha}(\text{eq})$ and the solute is surface active (adsorption of solute). Conversely, if $E_B > E_{\alpha}$ then solute interface desorption exists at equilibrium.

Several methods of calculating the solute interaction energy E_B for large-angle grain boundaries in single-phase systems have been reported(13,14). But if one assumes that the disordered structure of a random high-angle boundary resembles that of the liquid(15), then a natural extension is to set $E_B = E_L$ and $C_B(\text{eq}) = C_L(\text{eq})$ for a given temperature. For this case, equation (1.6a) may be rewritten as

$$E_B - E_S = kT \ln \left[\frac{C_S(\text{eq})}{C_L(\text{eq})} \right] = kT \ln [K(\text{eq})] \quad (1.6b)$$

where $K(\text{eq})$ is the equilibrium distribution coefficient (not to be confused with k which is Boltzmann's constant). $K(\text{eq})$ can be determined from the equilibrium phase diagram.

Turning our attention now to liquid-solid interfaces, a plausible assumption for allowing one to estimate E_B and the corresponding boundary segregation might be to:

assume the liquid-solid boundary to be disordered and similar to the liquid phase. Then $E_B \approx E_L$ and $C_B(\text{eq}) \approx C_L(\text{eq})$.

One possible means of experimentally determining E_B , at least semiquantitatively, for liquid-solid interfaces,

is to utilize the famous Gibbs(16) adsorption isotherm equation

$$\Gamma^B = - \left(\frac{\partial \sigma}{\partial \mu^B} \right)_{T,P} \quad (1.7)$$

or for when the solute composition is small

$$\Gamma^B = - \frac{1}{RT} \left(\frac{\partial \sigma}{\partial \ln C} \right)_{T,P} \quad (1.8)$$

Γ^B is the number of solute atoms adsorbed per unit inter-
face area, σ is the surface free energy per unit area, and
 μ^B and C are the solute chemical potential and composition
present in the system that are being adsorbed. From this
equation it is seen that if raising the solute composition
or chemical potential causes a reduction in the work σ
required to form a unit area of the surface, then Γ^B is
positive and solute is adsorbed by the interface. If
addition of solute increases σ then the solute species
will be rejected at the interface (desorption). Hence, if
 σ is experimentally measured as a function of $(\ln C)$ then
 Γ^B can be found. But Γ^B is the number of solute atoms
adsorbed per unit interface and not a composition at a
particular position in the interface. Nevertheless, from
 Γ^B the nature of the segregation can be determined and
also $C_B(\text{eq})$ and E_B (at the center plane of the interface)
can be estimated if one assumes a particular $E = E(x)$ or
 $C_B(\text{eq}) = C(x)$ for the boundary.

This method of characterizing solute equilibrium
segregation at interfaces by an interaction energy has

been used by Cahn(17) to develop a theory for boundary motion during recrystallization (see Section I.5). Cahn's approach will be extended in Chapter V to enable the partitioning at moving interfaces to be expressed as a function of growth velocity for binary alloy solidification.

I.4 Driving Force for Interface Motion in Binary Alloys

Before discussing interface motion in binary alloys it is worthwhile to comprehend the thermodynamic fundamentals which allow such a process to take place. At constant pressure for binary alloys the composition variable in addition to the temperature must be taken into account if the thermodynamics is to be understood. One can then predict when such a process is energetically possible and determine the driving force for the reaction if it does occur. These driving forces will be illustrated graphically.

In binary phases the chemical potentials (μ^A and μ^B) of A and B are defined(18)

$$\mu^i \equiv \left(\frac{\partial G}{\partial n^i} \right)_{T, P, n^j} \quad (1.9)$$

as the rate of change in the Gibbs free energy G when an i-th component is added at constant temperature and pressure. The two chemical potentials are related by the

Gibbs-Duhem equation, which for constant T and P is

$$(1 - C)d\mu^A + Cd\mu^B = 0 \quad (1.10)$$

where C is the mole fraction of B. This equation permits calculation of the chemical potential of one component from a knowledge of the other. The molar Gibbs free energy, $G_m = G/(N_A + N_B)$, is related to the chemical potentials by

$$G_m(C) = (1 - C)\mu^A(C) + C\mu^B(C) \quad (1.11)$$

and by use of the Gibbs-Duhem equation

$$\begin{aligned} \mu^A &= G_m - C\left(\frac{\partial G_m}{\partial C}\right) \\ \mu^B &= G_m + (1 - C)\left(\frac{\partial G_m}{\partial C}\right) \end{aligned} \quad (1.12)$$

Equation (1.9) expresses the important property of the chemical potential. It is the increase in free energy of the entire system when an infinitesimal amount of one component is added reversibly (per mole added). From this property we have the important condition that for equilibrium the chemical potential must everywhere have the same value. Equations (1.12) form the basis of the popular graphical methods of tangents(19). They express the fact that a tangent drawn to the molar free energy curve in Figure 1.1 at the composition of interest intercepts the $C = 0$ and $C = 1$ vertical axis at a value of G_m equal to

the chemical potential of the component. Hence a common tangent among two or more phases implies equality of chemical potentials and equilibrium (see Figure 1.2). A tangent to a G_m versus C curve also has an important meaning for reactions of a phase with composition change. The equation of a line tangent to G_m at $C = C_\alpha$ is

$$G_m(C, C_\alpha) = (1 - C)\mu^A(C_\alpha) + C\mu^B(C_\alpha) \quad (1.13)$$

If an infinitesimal amount of material of composition C were to be added reversibly to α of composition C_α , then $G_m(C, C_\alpha)$ would be the change in free energy of α per mole of material added as in Figure 1.3. Here C is the composition of material added. It may be quite different from C_α , the composition of α , which is the value of C where the line is tangent to the α free energy curve. The free energy change ΔG per mole reacted for diffusionless reactions of composition C_0 from α to β is obtained graphically in Figure 1.4 by reading the vertical distance between tangents at C_0 (incidentally the distance between tangents for the case coincides with the distance between curve to curve at C_0). Analytically the free energy changes per mole of β is

$$\Delta G_m = (1 - C_0)(\mu_\beta^A - \mu_\alpha^A) + C_0(\mu_\beta^B - \mu_\alpha^B) \quad (1.14)$$

The free energy change ΔG per mole β formed in a closed system that transfer small amounts of components from α at

composition C_α to β at a different composition of C_β is attained graphically in a similar way as before by reading the vertical distance between tangents at C_β (see Figure 1.5). This free energy change per mole β formed can be expressed if C_0 is changed to C_β in equation (1.14)

$$\Delta G = (1 - C_\beta)(\mu_\beta^A - \mu_\alpha^A) + C_\beta(\mu_\beta^B - \mu_\alpha^B) \quad (1.15)$$

This substitution is necessary because the free energy change desired is per mole β formed and β is no longer of composition C_0 .

To inquire if a solid can form from a single-phase liquid of composition C_0 one draws a tangent to G_L at C_0 and sees if the free energy curve of any solid phase lies below the tangent (see Figure 1.6).

The composition range over which G_S lies below the tangent gives the range of composition of solid that can form. At temperatures above the liquidus no solid can form. At the liquidus one solid just touches the tangent. It is the only solid that can form and it must form with the equilibrium composition. At lower temperatures an increasing range of solid compositions can form.

To take advantage of the isothermal aspects of the graphical methods this same range of solid compositions can be presented isothermally by varying the liquid composition C_L . At a given temperature the range of thermodynamically possible solid compositions C_S that can

form from a liquid of varying compositions C_L , is shown in Figure 1.7 as an area enclosed by the curve where $\Delta G = 0$ (OABEP). The right-hand most point on the curve E depicts the equilibrium compositions. The tangent to the liquid touches the solid only at one point (see tangent 1 in Figure 1.8). As the liquid composition moves to the left (tangent 2) the range of possible solid compositions at first increases and then decreases again.

The maximum solid composition ($C(T_0)$ in Figure 1.7, tangent 3 in Figure 1.8) is the composition where the two free-energy curves cross. Only one liquid composition, $C(T_0)$, can give this solid. If the liquid is either more or less supersaturated this maximum solid composition ceases to be possible. Diffusionless transformations, shown as a line OB of slope 1 in Figure 1.7, can only occur if the liquid composition is below this crossover composition(20). Following the usage in other transformations(21,22), we shall call the condition of equal free energies the T_0 condition and the composition $C(T_0)$. On a phase diagram T_0 forms a line between the liquidus and solidus lines. The line marks the upper limit to the liquid compositions and temperatures for diffusionless transformations. It also marks the upper limit to the compositions and temperatures of solid that can form isothermally from liquid of any composition.

Two other curves of thermodynamic interest are shown in Figure 1.7. These are the lines where chemical potentials of a component are equal in liquid and solid. For line OE, $\Delta\mu_B = 0$; for line PE, $\Delta\mu_A = 0$. Where the two lines cross we have equilibrium. These lines bound the regions of the figure where a particular component solidifies with a decrease in chemical potential. In the triangular region OEP both components would experience a decrease in chemical potential upon solidification. In this joint composition range the line tangent to the solid free energy versus composition curve lies everywhere below the line tangent to the liquid. Both components independently experience a decrease in free energy upon solidification. Outside the triangular region but within the $\Delta G = 0$ curve the tangent lines cross and although the overall free energy decreases upon solidification, one of the components experiences an increase in chemical potential. Solidification in this domain can only occur if the two species do not solidify completely independently of one another. One species enters the solid with an increase in its chemical potential because it is either passively trapped by the advancing solidification front or because it is a required participant in an independent solidification reaction mechanism involving several species which leads to an overall free energy decrease. In either case we will define "trapping" of a component to occur at an

interface when that species experiences an increase in chemical potential there.

It is worthwhile to describe the above conditions quantitatively for one simple case, that of dilute solution for both liquid and solid. Then the chemical potentials are given by Henry's Law for the minor component

$$\mu_S^B = B_S + RT \ln \gamma_S C_S \quad (1.16)$$

$$\mu_L^B = B_L + RT \ln \gamma_L C_L \quad (1.17)$$

where the B's and γ 's are related constants that depend on temperatures and reference states. We may eliminate the constants by noting that the chemical potentials are equal at equilibrium when $C_S = C_S(\text{eq})$ and $C_L = C_L(\text{eq})$, then the change in chemical potential across the solidification front is

$$\Delta\mu^B = \mu_S^B - \mu_L^B = RT \ln \frac{C_S C_L(\text{eq})}{C_S(\text{eq}) C_L} \quad (1.18)$$

In terms of the distribution coefficient K at the interface, defined as C_S/C_L , and its equilibrium value, $K(\text{eq}) = C_S(\text{eq})/C_L(\text{eq})$, this becomes

$$\Delta\mu^B = RT \ln [K/K(\text{eq})] \quad (1.19)$$

The minor component experiences no change in chemical potential when

$$C_S = K(\text{eq}) C_L \quad (1.20)$$

This is a straight line OE with slope $K(\text{eq})$ through the origin in Figure 1.7. When $K < K(\text{eq})$, $\Delta\mu^B < 0$. This is the region below the line OE. The area above line OE corresponds to "solute trapping". For the major component Raoult's Law hold and

$$\Delta\mu^A = RT \ln \frac{(1 - C_S)(1 - C_L(\text{eq}))}{(1 - C_S(\text{eq}))(1 - C_L)} \quad (1.21)$$

The major component experiences no change in chemical potential when

$$[C_S(\text{eq}) - C_S] = [1 - C_S(\text{eq})/1 - C_L(\text{eq})][C_L(\text{eq}) - C_L] \quad \dots\dots\dots (1.22)$$

This is a straight line PE of slope $[1 - C_S(\text{eq})]/[1 - C_L(\text{eq})] \approx 1$ through the equilibrium point $[C_S(\text{eq}), C_L(\text{eq})]$ in Figure 1.7. The regions above and below the PE corresponds respectively to $\Delta\mu^A$, less than or greater than zero. Solvent trapping would occur below PE.

The $\Delta G = 0$ curve is given by

$$(1 - C_S) \Delta\mu^A + C_S \Delta\mu^B = 0 \quad (1.23)$$

This curve must pass through the points O, B, E, and P.

1.5 Continuous Interface Motion in Binary Alloys

In Section 1.2 it was shown by Equation (1.1) that the response of an interface in pure materials (one component systems) to the conditions at the interface can

be expressed by

$$V = -M\Delta G \quad (1.1)$$

or in general, in terms of the variables V and T

$$f(V,T) = 0 \quad (1.24)$$

For binary systems the additional variable of composition must be taken into account and two interface response functions are needed to describe the interface motion. For an $\alpha \rightarrow \beta$ transformation these functions are

$$\begin{aligned} f_1(C_\alpha, C_\beta, V, T) &= 0 \\ f_2(C_\alpha, C_\beta, V, T) &= 0 \end{aligned} \quad (1.25)$$

where C_α and C_β are the solute interface compositions of the α and β phases. Such response functions could equally well be solved for the response, V and C_α , in terms of the temperature T and β interface composition C_β .

$$\begin{aligned} V &= g_1(T, C_\beta) \\ C_\alpha &= g_2(T, C_\beta) \end{aligned} \quad (1.26)$$

Such a form of the response functions are especially valuable when considering a solid state transformation under steady state conditions. For this case C_β is equal to the overall solute composition C_0 of the system and the temperature T is the imposed variable.

For steady state solidification the desired response functions are

$$\begin{aligned} T &= h_1(V, C_s) \\ C_L &= h_2(V, C_s) \end{aligned} \quad (1.27)$$

since $C_s = C_o$ and the growth velocity V is now a conveniently controllable parameter. It should be noted no matter which form of the response functions are chosen they describe the same relationship and are equivalent. From this view point it is readily evident that the principles of solidification are equivalent to those of interface motion during solid state transitions, and basic approaches applicable to one should be satisfactory for the other.

For solidification, due to the high diffusivities in the liquid and the usual comparatively small growth velocities, it is customary to assume the liquid and solid interface compositions are not substantially different from equilibrium compositions. Such a condition is called "local equilibrium" at the interface. The significance of this assumption is that the interface compositions are now independent of growth velocity V and dependent only on interface temperature T . For any temperature the liquid and solid compositions can be read from the liquidus and solidus lines on the equilibrium phase diagram; hence the response functions are known.

If the above assumption is not made two common approaches have been used to determine the response functions for the solidification process: Absolute reaction rate theory and irreversible thermodynamics.

A theory for determining the response functions for binary solidification using the absolute reaction rate approach has been developed by Jackson(23). It is an extension of the work by Jackson and Chalmers(12) to two component systems. Such an extension can easily be made since an inherent assumption of the previous work is that the atoms traverse the phase boundary individually. Hence the following convenient assumption of the Jackson theory was a natural one: the rate at which j atoms of each species leave a phase and traverse the interface is proportional to the mole fraction of the species in that phase. This assumption allows Jackson to develop an analysis which lends itself readily to physical interpretation. Details of this theory will be given in the next chapter.

The more popular approach to the problem for binary solidification has been through the use of irreversible thermodynamics. The starting point for these theories is by assuming a relationship similar to equation (1.1) for each atomic species, that is the flux of each species across the phase boundary is linearly proportional to the gradient of its chemical potential. A thorough analysis of these theories will be given in Chapter IV.

Since it is well known even traces of a second atomic species retards interface motion during recrystallization, Cahn(17) has formulated a theory to account for the interface drag of a second species on interface motion. It is assumed when the material is pure equation (1.1) is valid. When a solute species is present its drag on the interface is determined and in turn the resulting response functions can be found. The nature of the above solute effect depends on the magnitude of the solute interaction energy E_B relative to the interaction energy in the bulk phase. These are the same equilibrium solute interaction energies as found in equations (1.5) and (1.6a). An extension of this Solute Drag Theory to binary solidification is given in Chapter V. The necessity of this alternate approach to determine the interface partitioning during binary solidification was found to be needed since there are defects in the previous two methods. These deficiencies will be covered in Chapter IV.

I.6 Scope and Objective of Thesis

The purpose of this investigation is to make a detailed examination of the response of a solid-liquid interface to various conditions at the interface. Specifically, this study has been made to gain insight into the relationships between solute partitioning (solid and liquid interface compositions), the interface

temperature, and the growth rate during binary alloy solidification. Such relationships are called "response functions."

A knowledge of the response functions is of utmost importance in the field of solidification since they are needed boundary conditions to differential equations which are capable of describing the kinetics of solidification. Such a mathematical analysis in turn can help in predicting and controlling cast alloy properties.

If it is assumed that the interface is highly mobile, then even for small deviations from equilibrium the interface velocity is expected to be large. For this case it is expected that the solute partitioning should be a function of only the interface temperature and not dependent on the growth rate. Such a condition where the interface compositions are close to the equilibrium compositions is called "local equilibrium." Since most solidification studies are carried out at low velocities the condition of local equilibrium has gained wide acceptance as a valid form for the response functions. The first objective of this investigation is to test the validity of local equilibrium under extreme solidification conditions. In Chapter II it will be shown that compositions of a resulting solid after freezing were found to be larger than the stable or metastable solidus composition at any temperature and therefore a departure from local equilibrium at the

liquid-solid interface occurred. This investigation was performed by studying the zinc-rich solid phase in zinc-cadmium alloys after splat cooling. Chapter III will then concern itself with thermodynamics aspects of solidification when the solid composition lies in various regions of the equilibrium phase diagram.

With the above experiments in mind, previous theories on non-equilibrium partitioning are examined in Chapter IV. With the aid of the experimental results in the zinc-cadmium work, serious deficiencies have been found in each of these theories. Since most of these theories are irreversible thermodynamic in nature, special attention is given to this type of method and surprising conclusions are drawn. Chapter V will be concerned with attempting to overcome the above shortcomings by using the solute drag approach.

Before proceeding to the next chapter it should be noted that the major portion of Chapters II*, III**, and IV** have been published.

* J. C. Baker and J. W. Cahn, *Acta. Met.*, 17, 575, (1969).

** J. C. Baker and J. W. Cahn, "Solidification," *Amer. Soc. for Metals* (1970).

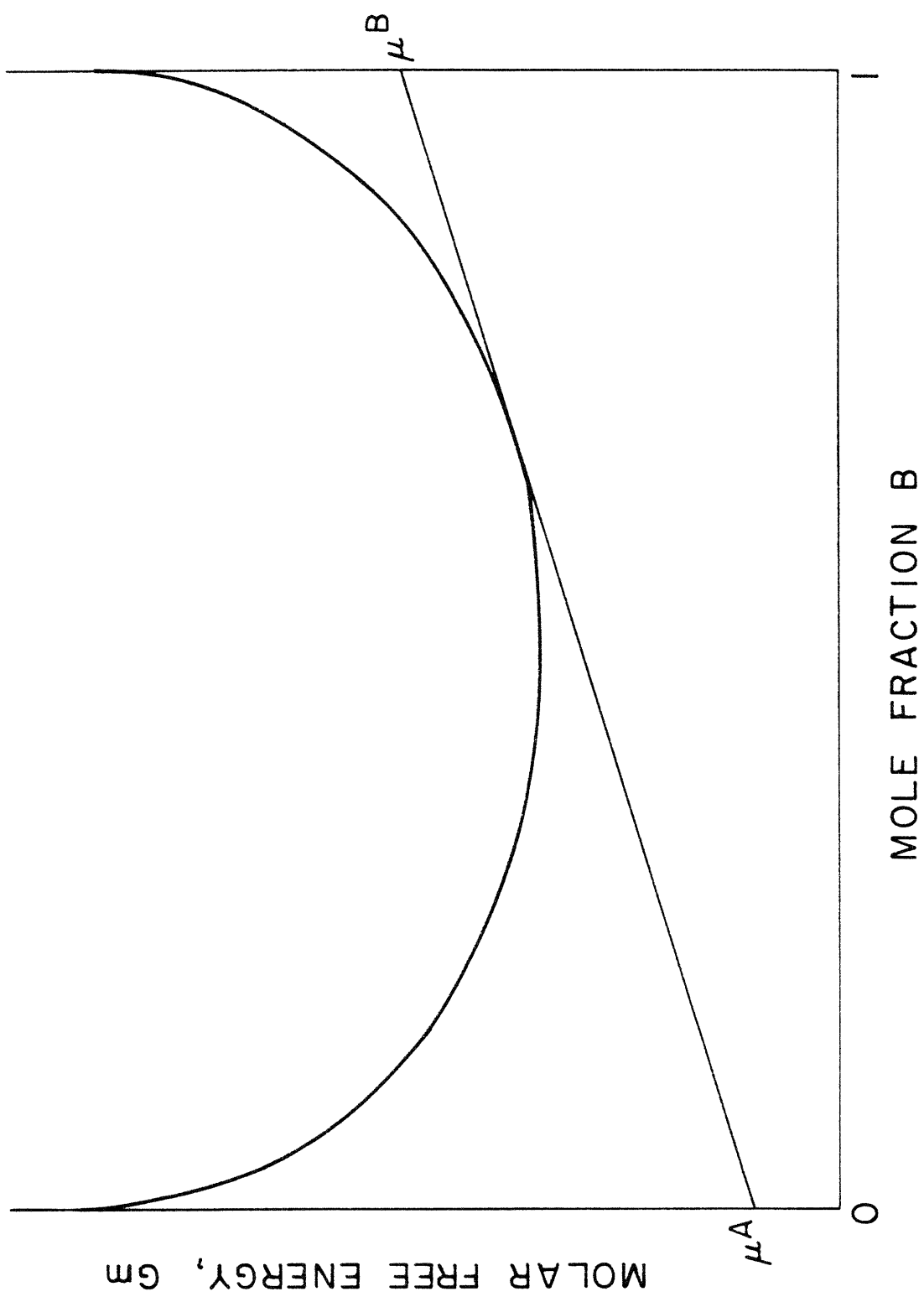
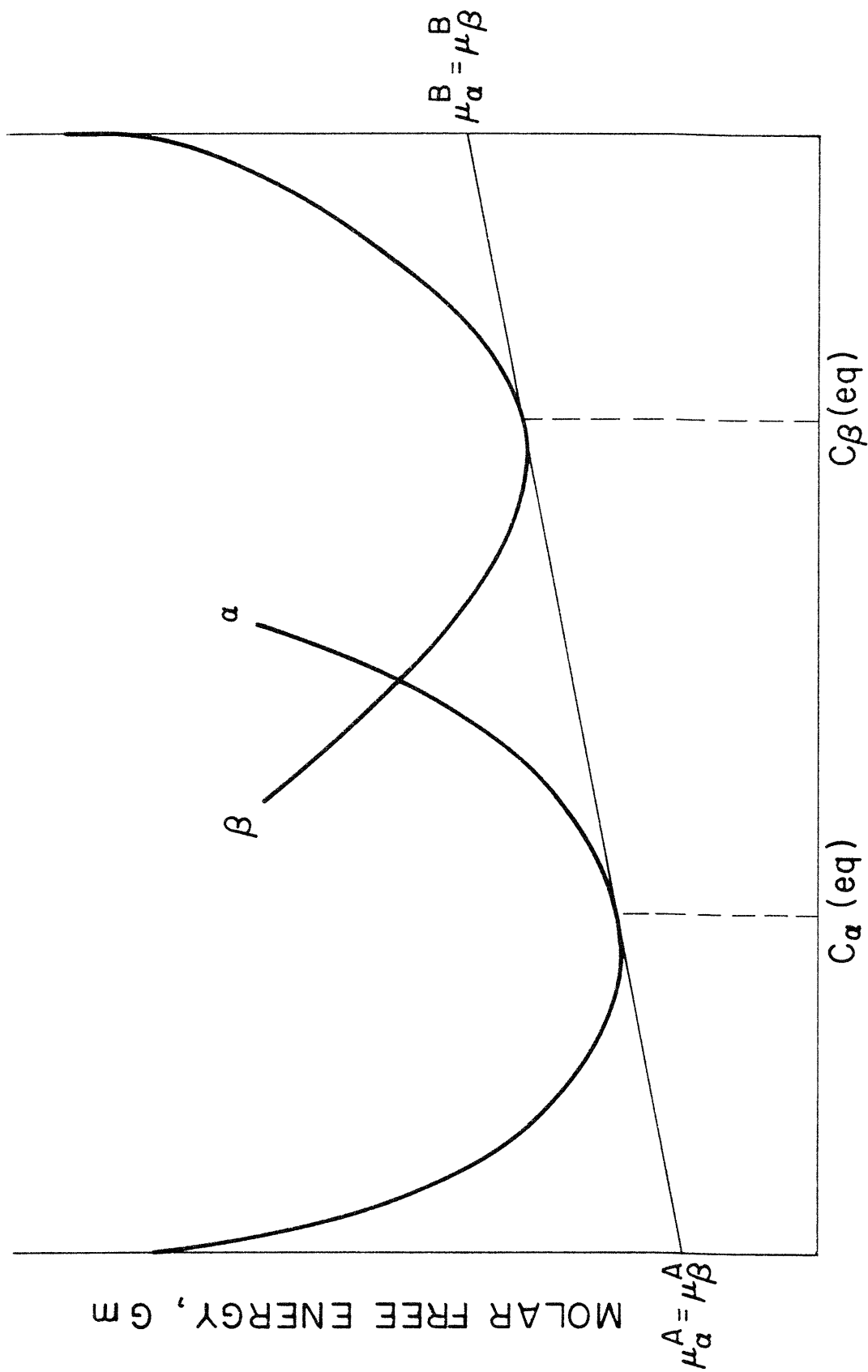
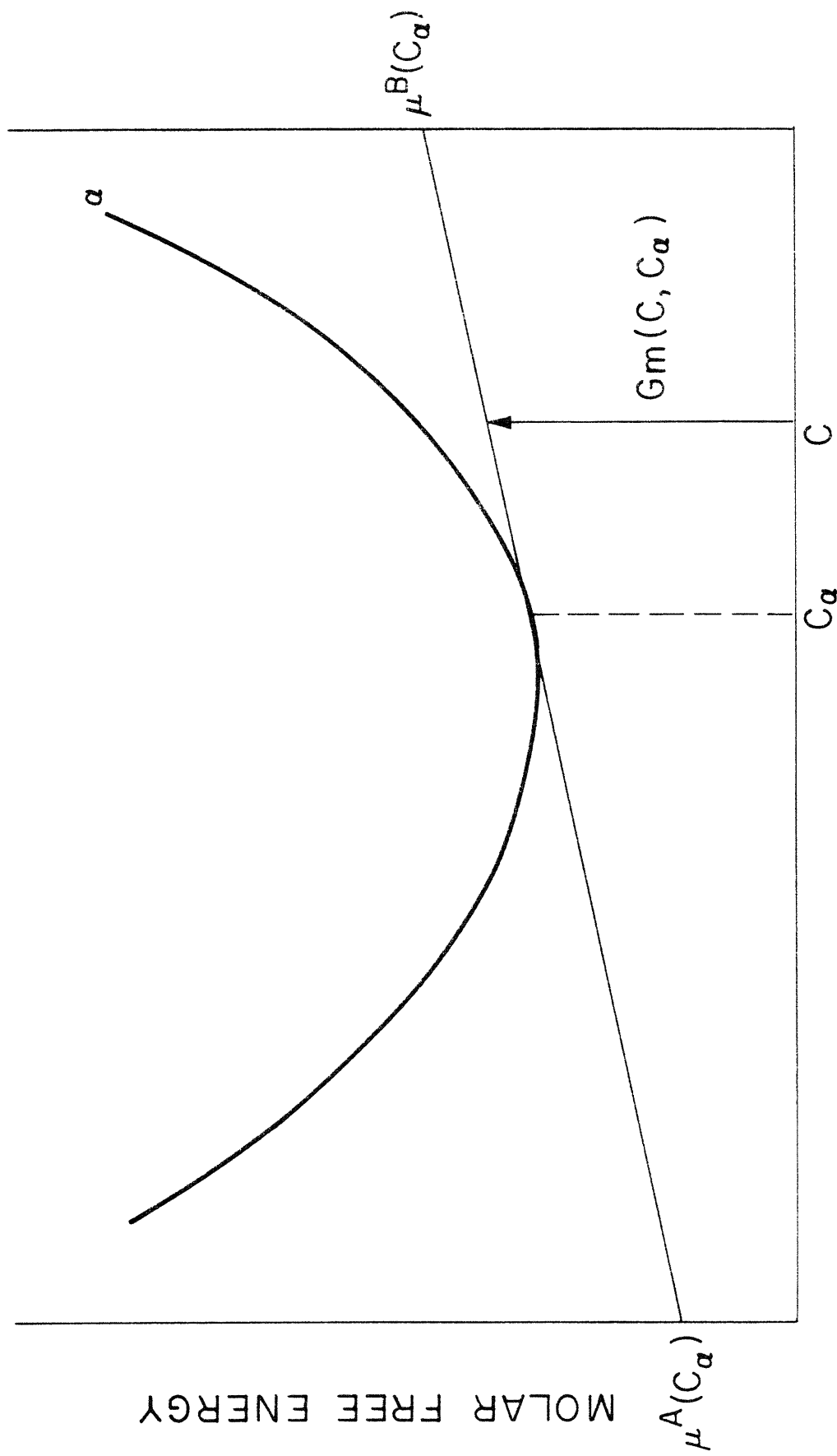


Figure I-1. Graphical method for obtaining the chemical potentials from the molar free energy curve.



MOLE FRACTION B

Figure I-2. Graphical construction for obtaining the equilibrium chemical potentials and compositions from the free energy curves for a binary system.



MOLE FRACTION B

Figure I-3. Graphical method for obtaining the total free energy charge of α when a mole of material of composition C is added to a large amount of α at composition C_α .

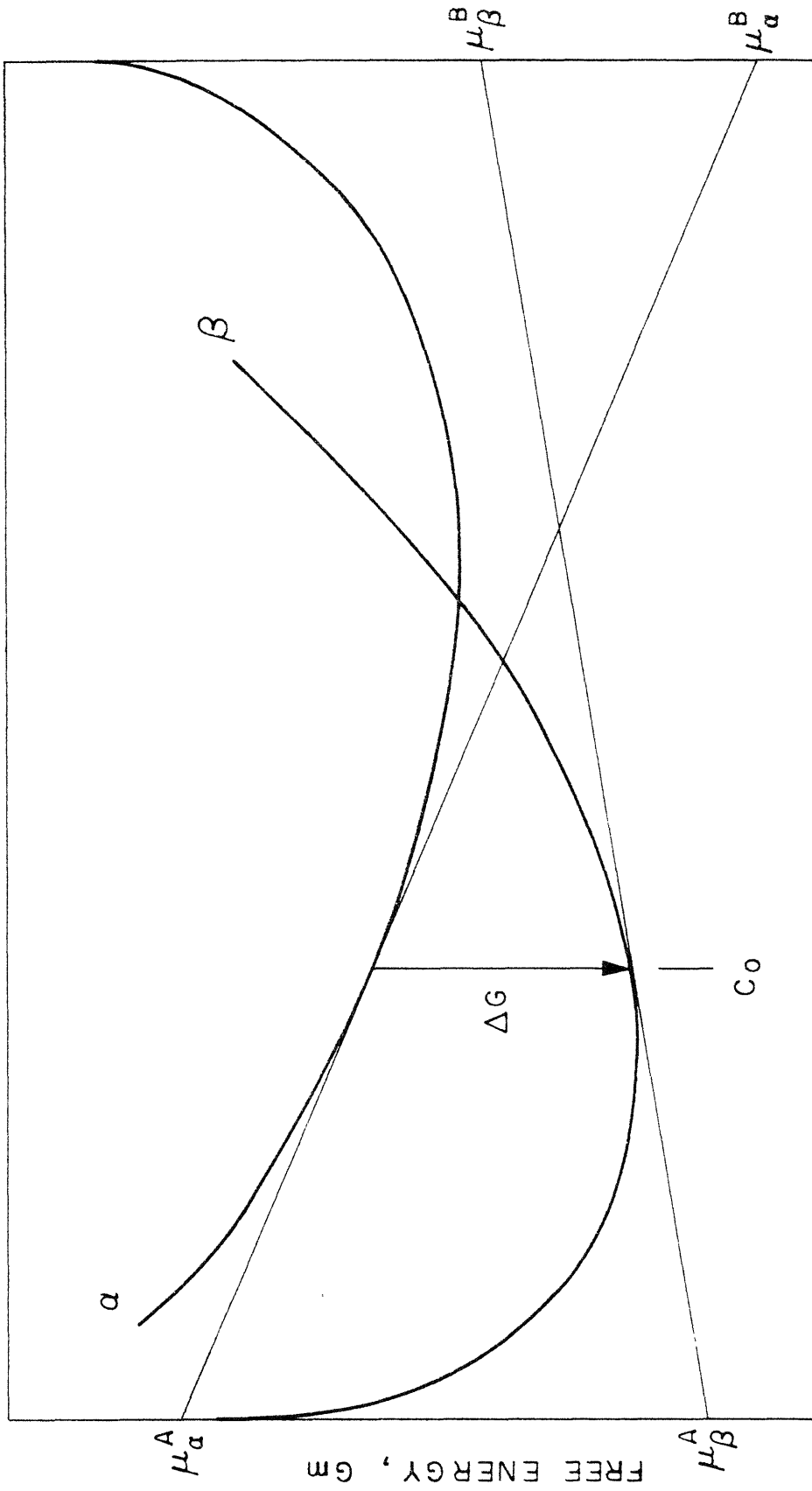
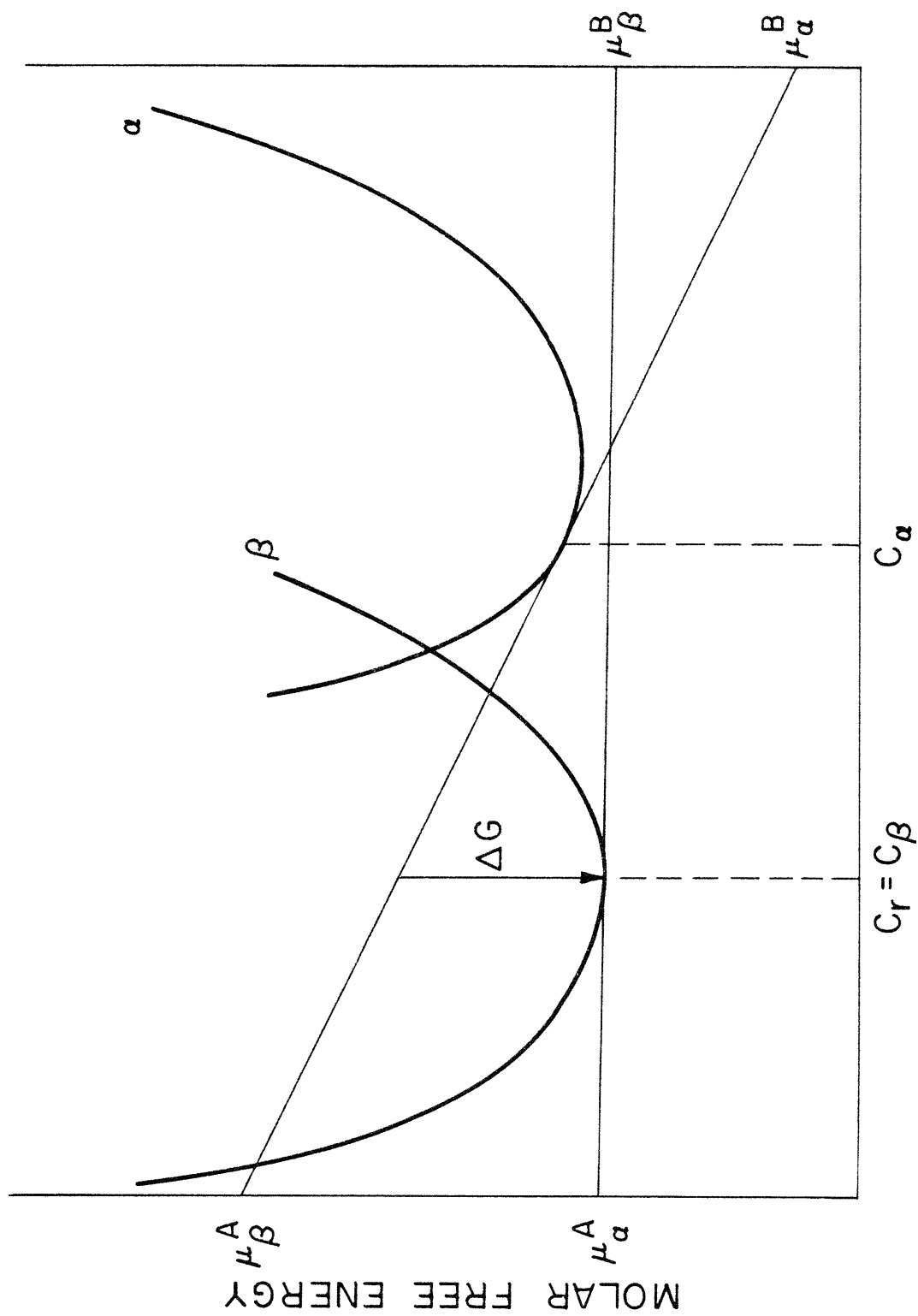


Figure I-4. Graphical illustration of free energy ΔG per mole reacted for diffusionless reactions of composition C_0 from α to β .



MOLE FRACTION B

Figure I-5. When the ratios of the reacting components coincide with those of one of the phases, the general tangent-to-tangent rule for obtaining free energy changes reduces to a tangent-to-curve rule. Here $C_r = C_\beta$.

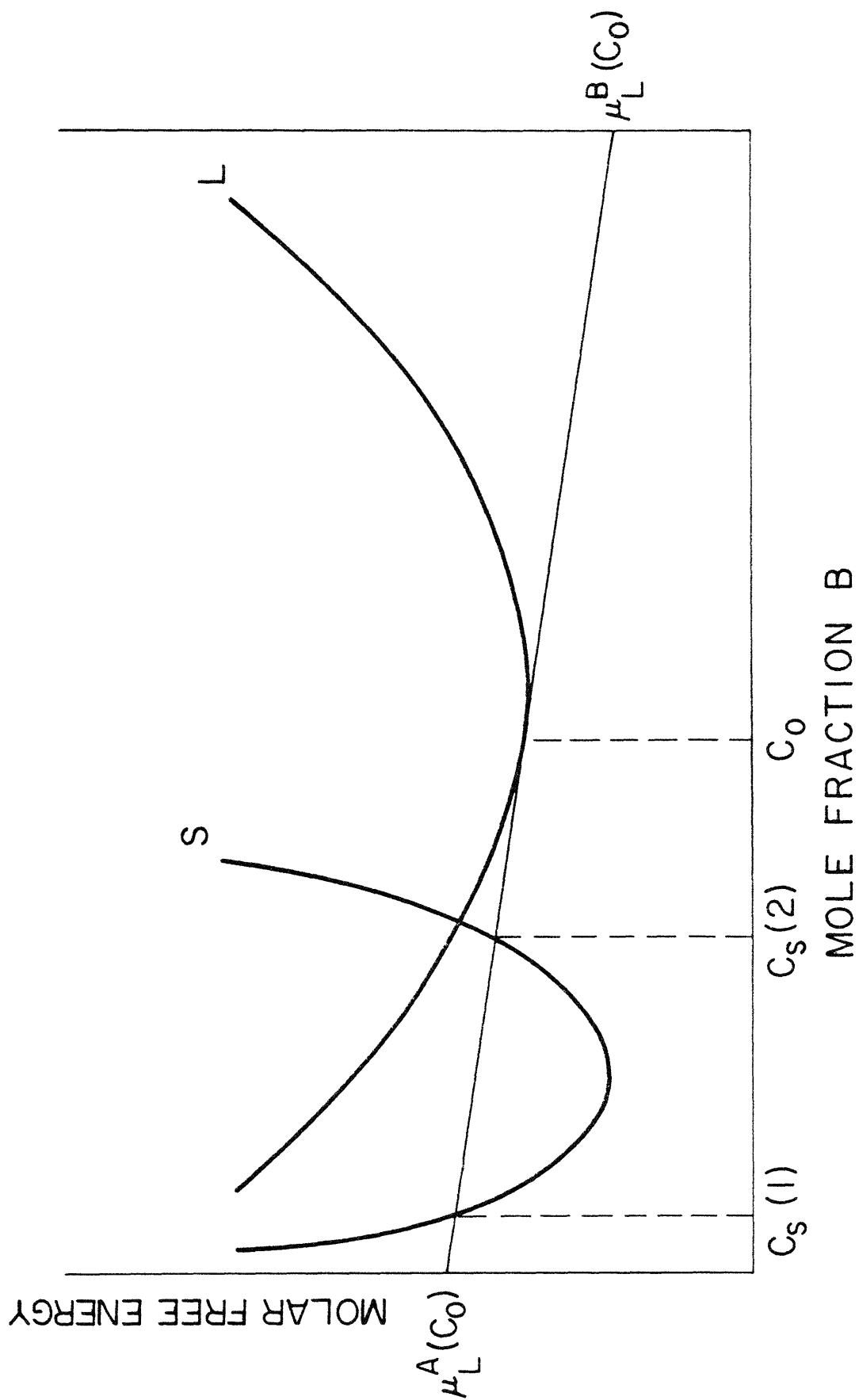


Figure I-6. It is thermodynamically possible to form solid of any composition between $C_s(1)$ to $C_s(2)$ from liquid of composition C_0 .

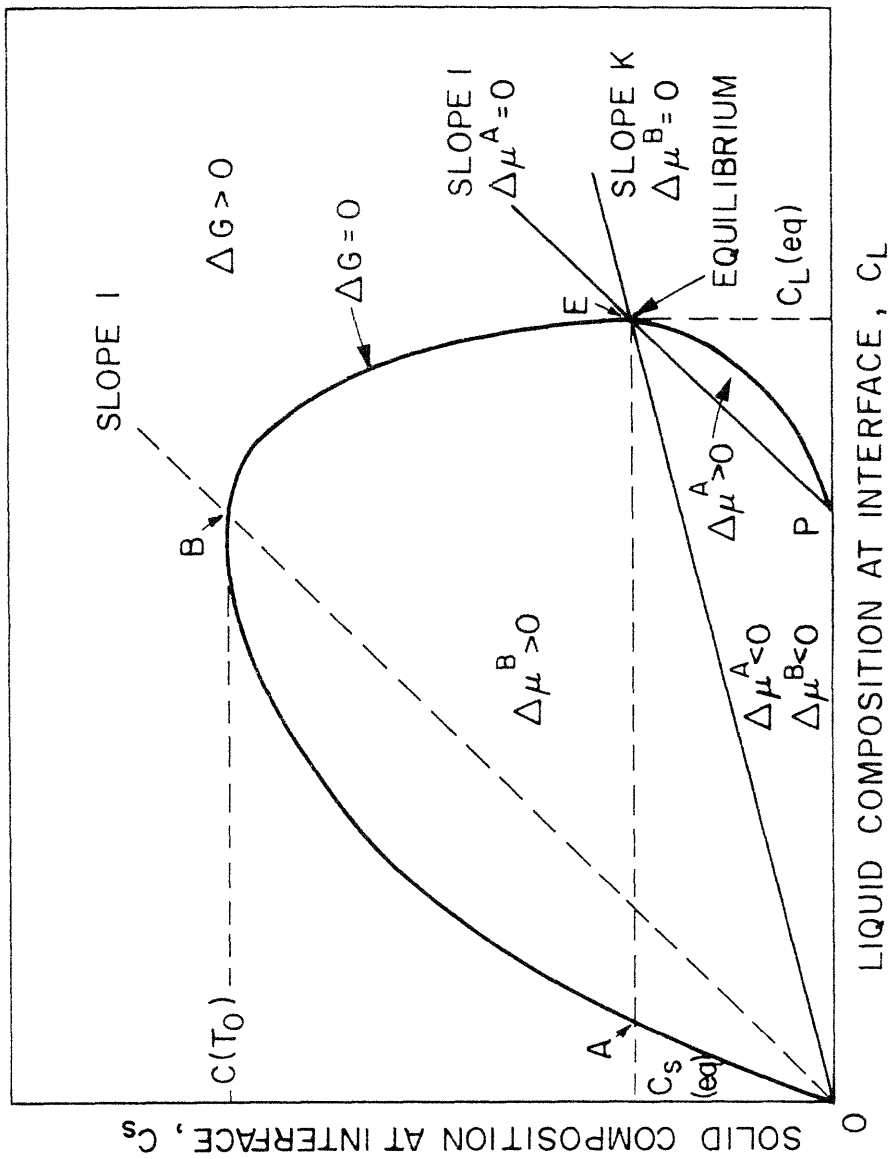


Figure I-7. The domain of all possible solid compositions that can form from various liquid compositions at a given temperature is enclosed within the curve OABEP. The curves OF and EP represent conditions of equal chemical potential for solute and solvent respectively. They are straight lines for dilute solutions. Their intersection E is the equilibrium condition. The line OB is for a diffusionless transformation, with B representing the T_0 condition.

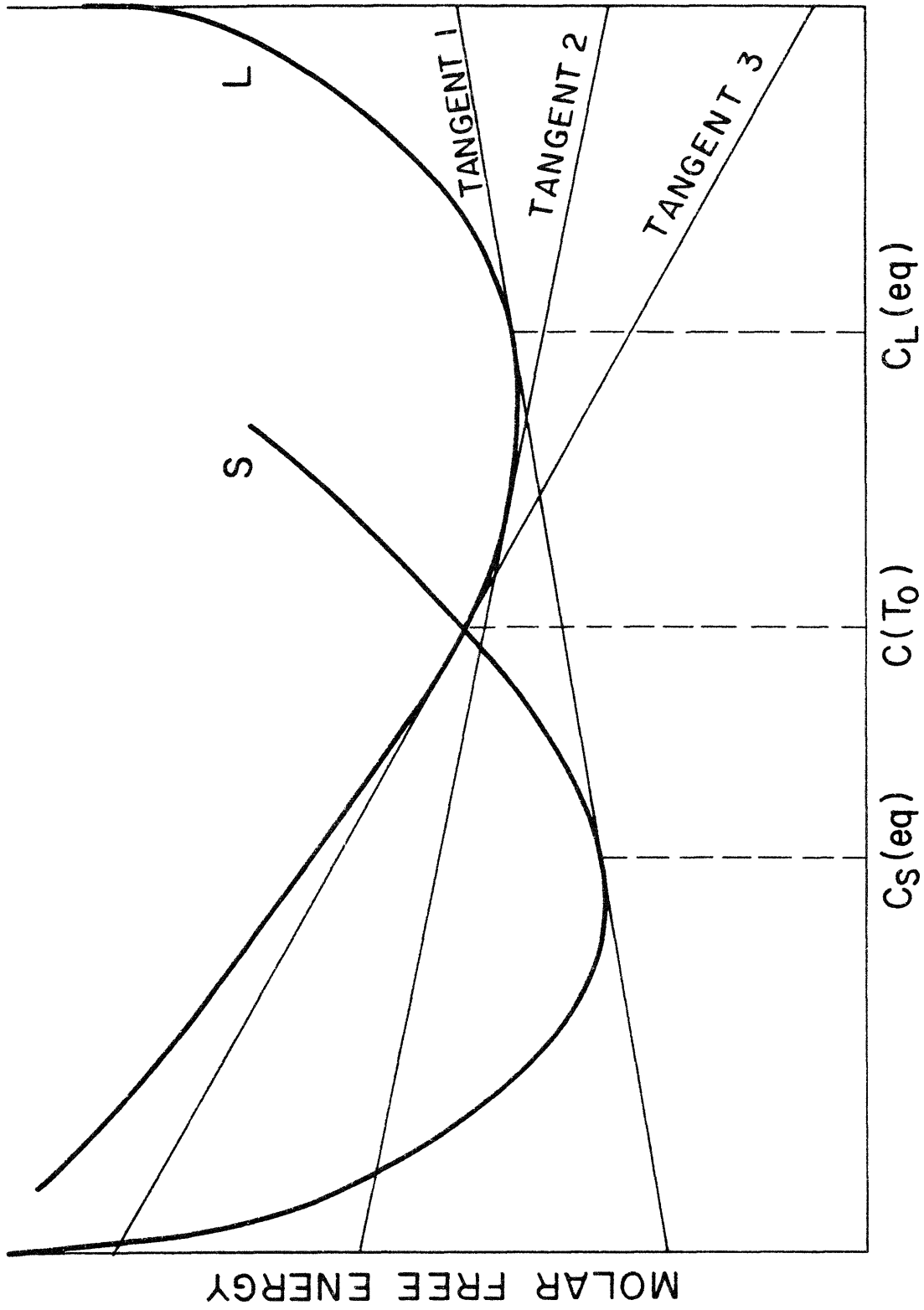


Figure I-8. Schematic free energy curves to illustrate the evolution of the curve OABEP of figure I-7.

Chapter II

SOLUTE TRAPPING BY RAPID SOLIDIFICATION

II.1 Introduction

Equilibrium between solid and liquid phases of metal alloys implies that the position of the phase boundary is fixed, i.e. the net rate of growth, V , is zero and that both phases are of uniform composition, but the compositions of the solid and melt are usually different. These equilibrium compositions are dependent on temperature; the possible compositions of solid and liquid correspond to two lines on the phase diagram, the solidus, below which in Figure 2.1 the solid is stable and the liquidus, above which the liquid is stable.

If the liquid-solid interface is allowed to move at a small rate (V_{small}), the solid and liquid phases need not be of uniform composition. But for all practical purposes, the solid phase at the interface can be assumed to be in equilibrium with the liquid at the interface ($C_S(i) = C_S(\text{eq})$ and $C_L(i) = C_L(\text{eq})$). In this thesis the above condition at the liquid-solid interface will be referred to as "local equilibrium."

For large growth rates it is questionable if the condition of local equilibrium at the interface holds. Consequently, the objectives of the investigation of this chapter are: (1) to obtain high growth rates by the method

of splat quenching and (2) to ascertain if there is a detectable departure from local equilibrium at the interface for the case of large growth rates.

If we measured the temperature at the liquid-solid interface during rapid solidification we would know the equilibrium composition of solid from the phase diagram for that temperature. Then we could check the validity of local equilibrium at the interface by comparing this equilibrium composition with the actual composition of the resulting solid. But it is a major experimental problem to determine the temperature at the crystallization front. If this temperature is unknown during the solidification, then for most alloy systems any observed solute redistribution can be rationalized from the assumption of local equilibrium at the interface, since the composition of the solid can be made to match a stable or metastable equilibrium solid composition by choosing the appropriate solidification temperature above or below the eutectic as indicated in Figure 2.2.

It is possible to avoid this problem of temperature determination by selecting an alloy system with a retrograde solidus (see Figure 2.3). The reasoning is as follows: since a retrograde system has a maximum in the solidus [$C_S(\text{eq max}) > C_S(\text{eq})$], if a composition of the actual solid can be measured which is greater than the retrograde maximum in the equilibrium solid composition [$C_S(i) > C_S(\text{eq max})$], a

positive departure from local equilibrium at the interface must have occurred [$C_S(i) > C_S(eq)$]. Hence, for this case we can measure a departure from local equilibrium without the temperature being known.

II.2 Experimental

The zinc-cadmium system was chosen for this investigation (see Figure 2.3). The solidus of the zinc-rich end of this alloy phase diagram was reported to be retrograde by Owen and Davies(24). The retrograde solidus was confirmed by the present author using X-ray lattice parameters to measure solid compositions at various temperatures. High-purity zinc (99.99%) and high-purity cadmium (99.99%) were sealed in an argon atmosphere in pyrex tubing, melted together, and quenched in water. Portions of these master alloys were then remelted and splat cooled to -196°C .

The shock-tube method of splat quenching of Duwez et al(25) was utilized. This technique employs a shock wave to eject liquid metal through a small hole in a crucible, atomizing the liquid in process. The liquid globules are rapidly spread on a copper substrate.

The resulting metal foils were kept at -196°C and analyzed on an X-ray diffractometer. Unit cell volumes (0.866 \AA^3) of the zinc-rich phase were calculated and plotted versus weight per cent cadmium of the initial liquid from zero to 5% (see Figure 2.4).

II.3 Discussion

The unit cell volume of the zinc-rich phase in Figure 2.4 can be considered as a measure of the concentration of cadmium in solid solution. Since we find that the unit cell volume is linear with respect to the composition of the initial liquid, we conclude that solid of compositions up to 5 wt. % cadmium have formed. The maximum composition of equilibrium solid in accordance with the retrograde phase diagram is 2.6 wt. % cadmium. Consequently, the solid solubility has been increased beyond the maximum solidus composition and a positive departure from local equilibrium at the liquid-solid interface has occurred in the solid composition, i.e. $C_S(i) > C_S(eq)$.

We are now in a position to compare the result of increasing the actual solid composition beyond the equilibrium composition of the solid with present theories. There are two basic types of theories that are shown invalid by this experiment; one by Jackson(23) is based on reaction rate theory, the second by Borisov(26) is a thermodynamic approach.

Let us first consider Jackson's kinetic description of alloy solidification. It is developed on the basis of two assumptions: (1) reaction rate theory can be applied independently to each species, and (2) the rate at which j atoms of each species leave a phase and traverse the

interface is proportional to the mole fraction of the species in that phase. From these two assumptions Jackson attains the equations for each atomic species

$$\begin{aligned} v_m^j &= K_m^j C_S^j(i) \\ v_F^j &= K_F^j C_L^j(i) \end{aligned} \tag{2.1}$$

where v_m^j is the rate at which atoms of the j species cross the interface to join the liquid, v_F^j is the rate at which j atoms cross the interface to join the solid, and $K^j = A^j G^j \sqrt{N^j} V^j \exp(-Q^j/RT)$ (in the notation of the cited paper) is a function of temperature but not of composition. The net rate of growth of each species is equal to the difference between v_F^j and v_m^j and is given by the equation

$$v^j = v_F^j - v_m^j \tag{2.2}$$

From equations (2.1) and (2.2) it can be shown Jackson's analysis predicts a negative deviation in local equilibrium for the solid at the interface, $C_S(i) < C_S(eq)$, which is contrary to the results of this investigation. The proof is as follows. For species B at equilibrium $v^B = 0$ and equation (2.2) becomes

$$v_F^B = v_m^B \tag{2.3}$$

Combining equations (2.3) and (2.1)

$$K_m^B C_S(\text{eq}) = K_F^B C_L(\text{eq}) \quad (2.4)$$

V^B is positive for solidification and is given by equation (2.2)

$$V^B = V_F^B - V_m^B \quad (2.5)$$

Combining equations (2.1) and (2.5) gives

$$V^B = K_F^B C_L(i) - K_m^B C_S(i) \quad (2.6)$$

and substituting for K_m^B from equation (2.4)

$$V^B = C_L(\text{eq}) K_F^B \left[\frac{C_L(i)}{C_L(\text{eq})} - \frac{C_S(i)}{C_S(\text{eq})} \right] > 0 \quad (2.7)$$

For solidification we must have a decrease in free energy, hence it can be easily shown any deviation from local equilibrium in the liquid composition is such that the liquid composition at the interface is less than the liquidus composition

$$C_L(i) < C_L(\text{eq}) \quad (2.8)$$

Equations (2.7) and (2.8) yield

$$C_S(i) < C_S(\text{eq}) \quad (2.9)$$

Hence, Jackson's theory predicts the wrong direction for the deviation from local equilibrium and the theory is invalid.

We now turn to Borisov's theory, which makes the thermodynamic assumption for a binary system that the chemical potentials of both species must decrease during solidification, i.e. the values of the chemical potentials at the interface must satisfy the following condition:

$$\begin{aligned}\mu_S^A(i) - \mu_L^A(i) &< 0 \\ \mu_S^B(i) - \mu_L^B(i) &< 0\end{aligned}\tag{2.10}$$

Equations (2.10) will now be shown to be inconsistent with the experimental results, $C_S(i) > C_S(eq)$, hence making Borisov's theory also incorrect.

At equilibrium for species B

$$\mu_L^B(eq) = \mu_S^B(eq)\tag{2.11}$$

Except at critical unmixing points and spinodals we have the following condition for each species in any stable or metastable phase

$$\partial\mu(i)/\partial C(i) > 0\tag{2.12}$$

For solidification with a decrease in free energy equation (2.8) holds true and when combined with equation (2.12) gives

$$\mu_L^B(eq) > \mu_L^B(i)\tag{2.13}$$

From our experimental result, $C_S(i) > C_S(eq)$, and equation (2.12)

$$\mu_S^B(i) > \mu_S^B(eq) \quad (2.14)$$

Combining equations (2.11), (2.13), and (2.14)

$$\mu_S^B(i) - \mu_L^B(i) > 0 \quad (2.15)$$

Therefore, the assumption of equations (2.10) and Borisov's theory are invalid.

It should be pointed out that equations (2.10) are not necessary thermodynamic conditions for solidification. The thermodynamic requirement is $\Delta G < 0$ for the overall transition. This permits $\Delta\mu > 0$ for one of the species.

It is now of interest to see why theories like Jackson's and Borisov's fail to agree with our experimental result. Both types of theories make the inherent assumption that some spontaneous activity is required of each species during solidification. The atoms that do not traverse to the solid are inactive. Thus each species must lower its free energy on solidification. Experimentally we find that the cadmium atoms experience an increase in chemical potential. This means that if the cadmium atoms could act independently they would attempt to avoid the solid. During the time the cadmium's potential is being raised it must be passive. The cadmium is trapped in the solid by the solidification front and if it could have been active it would have remained in the liquid.

There is one atomistic theory which has in it the basic passivity of the solute and which therefore predicts the correct deviation in solid composition from local equilibrium. This is Chernov's theory (27) for the trapping of surface active solute atoms. These solute atoms seek the interface and are subsequently buried as the next layer of the crystal grows. It is during the burying that they are passive and their chemical potential is raised. If they can diffuse they attempt to remain in the surface.

The author believes Chernov predicts the correct departure because it is inherent in his beginning assumptions and not a product of the solution to his diffusion equation. The disputed assumption is: the initial composition of the new solid layer is identical to the interface layer from which it formed. Any later change in composition of this solid is then due to diffusion in the solid. Hence, for a surface active solute species this total initial capture of solute atoms is independent of the layer's lateral growth and neglects solute escape by interface diffusion ahead of the moving layer (the author feels this may be an important effect especially at small layer growths).

An analysis believed to be more realistic than the one above is given in Chapter V. It also predicts a positive deviation in solid composition from local equilibrium when the solute atoms are surface active.

II.4 Appendix

A. Verification of the Retrograde Solidus in Zinc-Cadmium

The validity of the conclusion of this experiment requires that the solidus including its metastable extension below the eutectic never exceeds the composition value at the retrograde maximum. But theoretical and experimental tests were performed to check that the solidus indeed has a maximum, and the metastable extension was shown theoretically to continue to decrease monotonically.

The various equilibrium solidus compositions were calculated by utilizing available thermodynamic data from the literature (28) and the following expression derived by Thurmond and Struthers (29).

$$\ln \left[\frac{C_s(\text{eq})}{C_L(\text{eq})} \right] = \frac{(\Delta H_f^B + \overline{\Delta H}_L^B) - \overline{\Delta H}_S^B}{RT} - \frac{\Delta S_f^B}{R} \quad (2.16)$$

Both the liquid and solid solutions are assumed to be regular solutions. ΔH_f^B and ΔS_f^B are the heat of fusion and entropy of fusion at the melting point of solute B, $\overline{\Delta H}_S^B$ and $\overline{\Delta H}_L^B$ are the differential heat of solutions of the solute in the solid and liquid phases. For regular solutions the above three ΔH 's and ΔS_f^B are constant. For the zinc-rich side in the Zn-Cd system they are (28):

$$\Delta H_f^{Cd} = 1530 \text{ cal.} \quad \overline{\Delta H_L^{Cd}} = 2015 \text{ cal.}$$

$$\Delta S_f^{Cd} = 2.58 \text{ cal/}^\circ\text{K.} \quad \overline{\Delta H_S^{Cs}} = 6904 \text{ cal.}$$

Using $C_L(\text{eq})$ values from the phase diagram, $C_S(\text{eq})$ values have been calculated at the temperature where the experimentally determined phase diagram predicts a maximum (600°K) and at the eutectic temperature (539°K). The two calculated solidus compositions are 1.30 at/o (at 600°K) and 1.23 at/o (at 539°K). Hence, these two composition values predict a retrograde solidus, and are in close agreement with the equilibrium phase diagram values (24) of 1.39 at/o and 1.20 at/o.

Let us now study equation (2.16) in detail for the Zn-Cd system. Whenever

$$\overline{\Delta H_S^B} \gg (\Delta H_f^B + \overline{\Delta H_L^B}) \quad (2.17)$$

the right-hand side of equation (2.16) is always negative and increases in absolute magnitude as the temperature T decreases. The above implies $\ln[C_S(\text{eq})/C_L(\text{eq})] \rightarrow -\infty$ and $C_S(\text{eq}) \rightarrow 0$ as the temperature T tends toward zero degrees Kelvin. For the zinc-cadmium system expression (2.17) is obeyed strongly. So strongly that heat capacity differences cannot produce appreciable changes in it. Hence, below the eutectic temperature the metastable equilibrium solidus compositions will continue to decrease with decreasing temperature.

For a maximum to occur in the stable portion of a solidus, it is desired that $\overline{\Delta H}_S^B$ and $[T_m^A - T_{\text{(eutectic)}}]$ be large. For systems where $\overline{\Delta H}_S^B < (\Delta H_f^B + \overline{\Delta H}_L^B)$ the solidus cannot have a retrograde maximum at any temperature.

The maximum in the solidus was checked experimentally by X-ray lattice parameter measurements. First, alloys of 3.5 w/o Cd were heated into the two phase liquid-solid phase diagram region and were allowed to equilibrate at the supposed temperature where $C_S(\text{eq})$ is a maximum and at a lower temperature. Both specimens were quenched in water and examined by X-ray lattice parameter measurements at -196°C . It was found that the specimen with the higher equilibration temperature had a larger unit cell volume at -196°C and hence was of higher composition. This in turn supports the retrograde nature of the solidus.

B. Verification of Presence of Only a Single Solid Phase

The second precaution was to examine the various splat cooled alloys by transmission electron microscopy. The test was to determine if only the zinc-rich β phase in Figure II.3 was present as indicated by X-ray analysis, or if the cadmium-rich α phase was also present in small amounts. If the β -phase is the only phase present when alloy compositions greater than $C_S(\text{eq})$ maximum are splat cooled, then all the cadmium is in solution in the β phase and $C_S > C_S(\text{eq})$. This is what was found by the

transmission electron microscopy (see Figure II.5). Only one phase appears to be present and the grain boundaries are clean.

If α phase particles had been found, it does not invalidate the experimental conclusion that $C_s > C_s(\text{eq})$. But the actual finding of no α phase present does support the conclusion that the composition of cadmium in solution is greater than the equilibrium composition.

One would expect if the cooling rate was decreased sufficiently, the system would tend toward equilibrium during the freezing process and form both β and α phases. The necessary segregation needed for the formation of these two phases most likely would occur by dendritic solidification. Figure II.6 is a micrograph of a replica of the surface of a Zn-3.5 w/o Cd alloy cooled by the piston and anvil technique(30). The specimen appears to consist of β dendrites and α interdendritic particles. The rate of cooling in the piston and anvil technique(30) is believed to be 10^5 ($^{\circ}\text{C}/\text{sec}$), where as the splat cooling methods leads to a cooling rate of approximately 10^7 ($^{\circ}\text{C}/\text{sec}$).

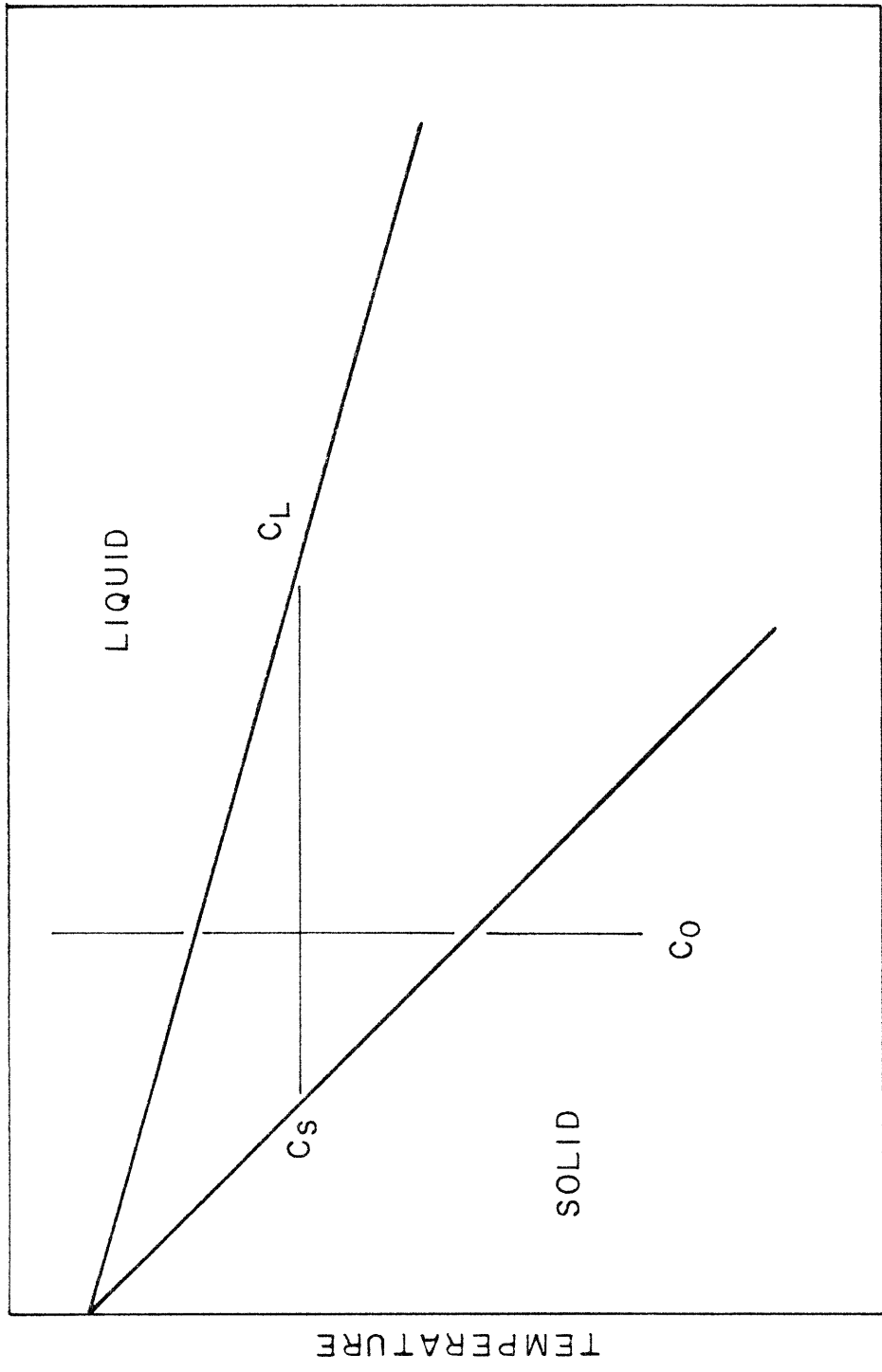


Figure II-1. Portion of phase diagram showing equilibrium composition of solid and liquid.

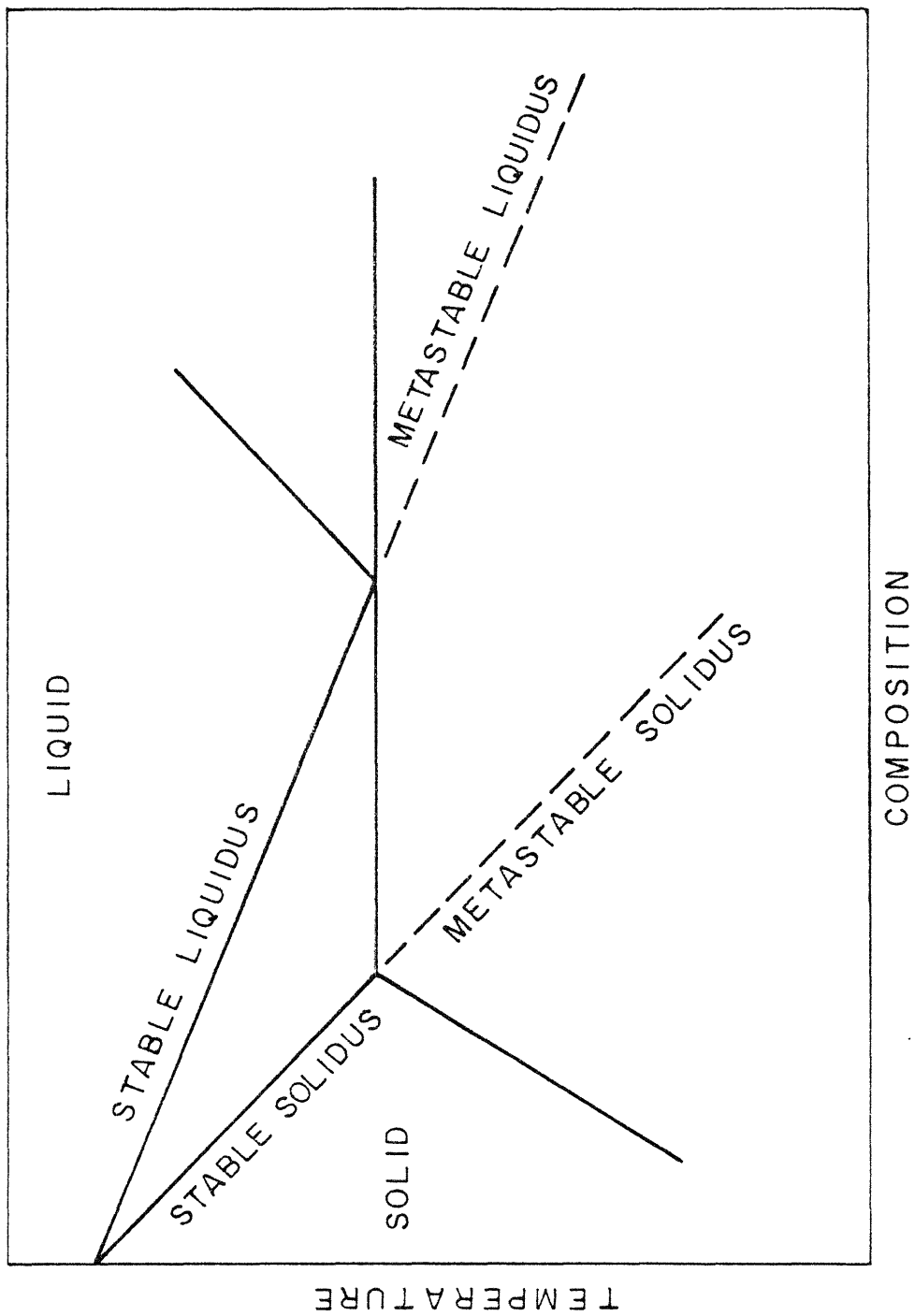


Figure II-2. Portion of eutectic phase diagram illustrating equilibrium metastability of solid and liquid.

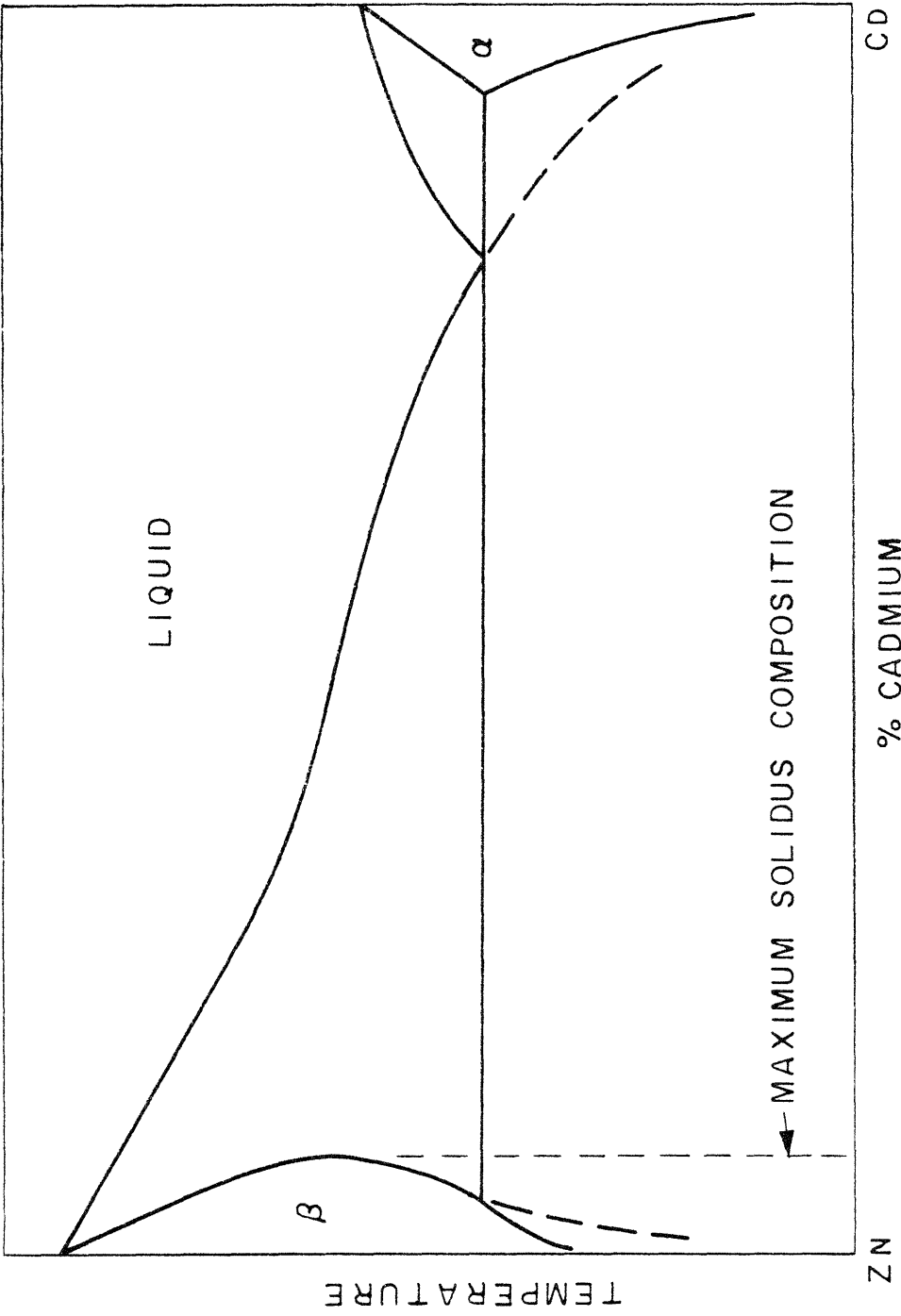


Figure II-3. Zinc-cadmium retrograde phase diagram.

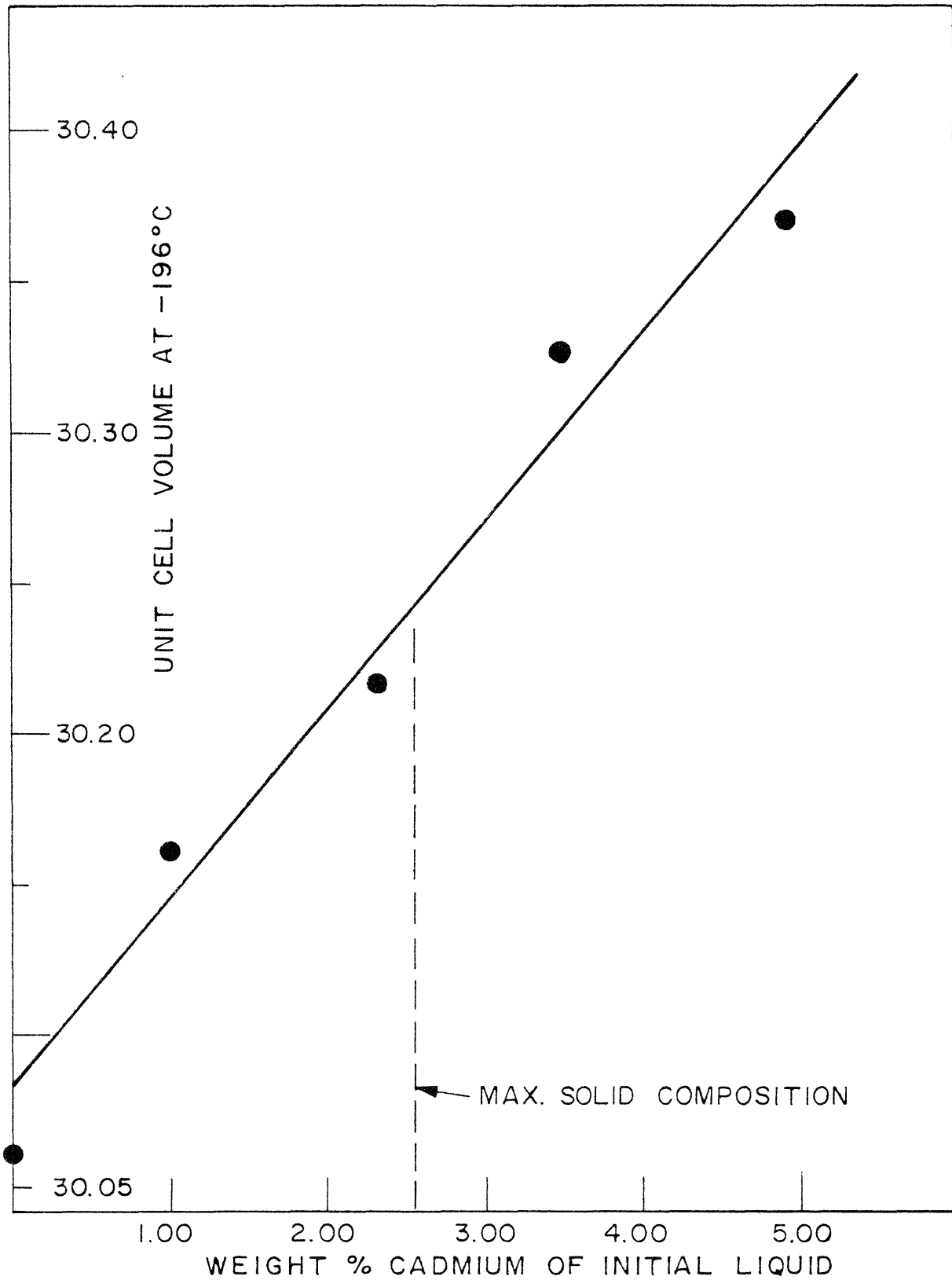


Figure II-4. Plot of unit cell volume of zinc-rich solid at -196°C against weight per cent cadmium of initial liquid.



Figure II-5. Electron micrograph of Zn -3.5w/o Cd which was splat quenched to -196°C . 130,000X.

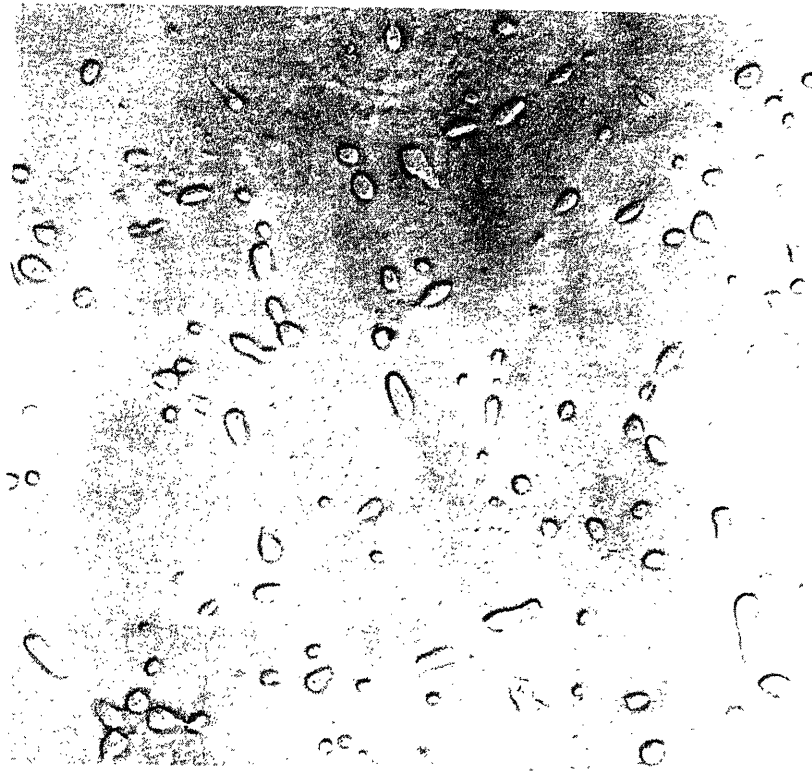


Figure II-6. Electron micrograph of replica of Zn -3.5w/o Cd which was cooled by the piston and anvil technique. 8,000X.

Chapter III

THERMODYNAMIC ASPECTS OF SOLIDIFICATION PROBLEMS

III.1 Introduction

The mathematical analysis of an N-component solidification problem with one solid phase consists of setting up $2N$ differential equations; 2 for heat flow and $(2N-2)$ for interdiffusion in the two phases. In addition the initial conditions and the boundary conditions must be given. Of these, $(2N+2)$ boundary conditions pertain to the liquid-solid interface. The reason this number of boundary conditions are needed is that the interface is not at a fixed position and additional conditions are needed to specify the interface velocity. The interface boundary conditions are:

(1) Continuity of temperature. It is believed that the heat transfer across the interface is sufficiently rapid that even in the most extreme heat fluxes temperature remains continuous across the interface.

(2) Conservation of heat. This condition includes a term for the latent heat of fusion L_m and thus involves the velocity V

$$K_S (\nabla T \cdot n)_S - K_L (\nabla T \cdot n)_L = L_m V \quad (3.1)$$

(3) N conservation of mass equations; one for each component

$$D_S (\nabla C \cdot n)_S - D_L (\nabla C \cdot n)_L = (C_S - C_L)V \quad (3.2)$$

These also contain the velocity.

(4) N "response" functions which describe the response of the interface to the conditions at the interface. These would give N quantities, e.g. the velocity of the interface and the composition of the solid, in terms of the instantaneous conditions; the interface temperature, the composition of the liquid, and the orientation and defect structure of the interface. This section will consider the thermodynamic aspects of these response functions.

For a single component system if we ignore the last three factors, such a response function would be

$$f(V, \Delta T) = 0 \quad (3.3)$$

or equivalently when solved for either V or ΔT

$$\begin{aligned} V &= g(\Delta T) \\ \Delta T &= h(V) \end{aligned} \quad (3.4)$$

All three equations express the same relationship and should be fully equivalent. If we impose a velocity and note the interface temperature and then in another

experiment apply this ΔT we should observe that the system responds with the same V .

For a binary system the two response functions would be

$$\begin{aligned} f_1(C_L, C_S, V, T) &= 0 \\ f_2(C_L, C_S, V, T) &= 0 \end{aligned} \tag{3.5}$$

which might be solved for the response, V and C_S , in terms of the interface temperature T and C_L

$$\begin{aligned} V &= g_1(T, C_L) \\ C_S &= g_2(T, C_L) \end{aligned} \tag{3.6}$$

Such a response function could equally well be expressed in terms of the compositions that would be found for a given T and V .

$$\begin{aligned} C_S &= m_1(T, V) \\ C_L &= m_2(T, V) \end{aligned} \tag{3.7}$$

As we shall see this form is convenient from a thermodynamic point of view. Another way of expressing the response functions would be to express the temperature T and C_L in terms of a given V and C_S

$$\begin{aligned}
 T &= h_1(V, C_s) \\
 C_L &= h_2(V, C_s)
 \end{aligned}
 \tag{3.8}$$

This is a valuable form for steady state solidification. These four ways of expressing the response function are fully equivalent to each other and an experimental determination of one form should be adequate for reexpression in all the other forms. Because they are boundary conditions to differential equations one form or another may be convenient for a particular experimental geometry but for a particular system the relations should be universal.

Thermodynamics places only general restriction on the response functions. It does not specify them. For the single component it specifies that the sign of V be related to the sign of ΔT . For the binary system it specifies only that for a given T , solidification ($V > 0$) requires that C_s and C_L lie inside or on the boundary of the curve OABEP of Figure 1.7. For purposes of mathematical analysis such a general restriction is insufficiently precise. We have to know more about the response functions.

Because these response functions are boundary conditions to a solidification problem it is difficult to perform experiments that isolate them sufficiently clearly. Ideally interface compositions, temperature, and velocity should be measured directly. Even in the single component

system the interface temperature is often inferred from bath temperatures with or without a heat flow correction. In multicomponent systems as we shall discuss, equilibrium at the interface is usually assumed(31) without even an attempt at experimental verification.

III.2 The Assumption of Local Equilibrium

If we assume that the boundary is so mobile that V is large for any deviation from equilibrium, the response functions become the conditions for local equilibrium, of which there also are N in number. Hence, for one component

$$\Delta T = 0 \quad \text{for all } V \quad (3.9)$$

and for two components the compositions at the interface are

$$\begin{aligned} C_S &= C_S(\text{eq}) = m_1(T, 0) \\ C_L &= C_L(\text{eq}) = m_2(T, 0) \quad \text{for all } V. \end{aligned} \quad (3.10)$$

The assumption is valid whenever the deviation from equilibrium, expressed as ΔT , $C_S - C_S(\text{eq})$, or $C_L - C_L(\text{eq})$ is small compared to the total temperature and composition ranges in the problem. Although the velocity V no longer appears in these conditions, it still appears in the conservation conditions (2) and (3), and the mathematical analysis can proceed.

The popularity of local equilibrium as an assumption rests on its expected widespread validity for most solidification problems which involve rather low interface velocities, and the fact that it gives a form to the response function that permits one to begin calculation of solidification problems. The test of the validity of the assumption could come from two kinds of experiments: the simultaneous measurement of all the interface variables or checking the applicability of predictions of calculations made using the assumptions. The former test has never been made and the latter test is most usually made qualitatively.

Qualitative predictions from the assumption can only show consistency or inconsistency. For instance we can, by using the assumption of local equilibrium, predict an enhancement of solid solubility in a eutectic beyond the maximum phase diagram value simply by invoking the assumption that the eutectic has been suppressed and solidification proceeds on metastable liquidus and solidus extensions below the eutectic. (Figure 3.1) However unless we simultaneously measure the interface temperature, we will not know whether we produced a deviation from local equilibrium or actually suppressed the eutectic reaction. Thus even the enhanced solubility produced by rapid solidification is by itself inadequate to prove that a significant deviation from local equilibrium was produced because the metastable solidus usually continues to

increase in composition. In the Zn-Cd system which has a retrograde solidus, the equilibrium solid solubility has a true maximum and the metastable extension continues to lower compositions. The maximum was exceeded by rapid solidification indicating that under extreme conditions the significant deviations from local equilibrium can be produced as shown in Chapter II.

It is interesting to note another case where local equilibrium ceases to exist during solidification. Even though the equilibrium shape of a crystal may be faceted, when originated during solidification the faceting is usually a result of the growth kinetics. Since such shapes are not solutions to the differential equations, the condition of local equilibrium at the interface does not hold. For instance, Glicksman and Vold(32) found faceting during the freezing of Bi at small velocities, but rounding of the interface during melting at small growth rates; this indicates an inconsistency with the condition of local equilibrium at the interface.

III.3 Steady-State Binary Solidification

Of the various experimental and theoretical methods of dealing with solidification the steady-state plane-front condition is an exceptionally useful one. We impose a velocity V on the system and assume that after an initial

transient the temperature and composition profiles and the position of the interface will move with the velocity V . Under these conditions the composition of the solid C_s must be equal to the alloy's overall composition C_o

$$C_s = C_o \quad (3.11)$$

Because $C_s = C_o$ the process has some aspects of "diffusionless" solidification, but it is highly likely that there will be a diffusional layer ahead of the interface and the composition of liquid at the interface C_L will differ from C_o . Under steady-state conditions this layer remains unchanged with time and may be hard to detect. It will have a thickness of order D_L/V , or less than 1μ when V exceeds 1 cm/sec. (33).

A study of steady-state solidification thus permits us to fix V and C_s and if we determine experimentally the value of T and C_L at the interface we would be evaluating the response functions. The functions although evaluated by a steady-state experiment should be universally valid for other geometries in that system. If in a non-steady state experiment the interface found itself with the same value of T and C_L as found in the steady-state experiment, it should respond with the same V and C_s .

Figure 3.2 shows Figure 1.7 redrawn for purposes of steady-state solidification. The horizontal line

represents the alloy composition that is equal to C_s . The possible values of C_L are those that lie on the horizontal line but within the curve OABEP appropriate for that temperature. The OABEP curves are given for the various temperatures, each representing a temperature lying within three distinct regions of the phase diagram given in Figure 3.3. Let us now examine steady-state solidification of an alloy of composition $C_o = C_s$ and investigate the possibilities and the phenomena that we would encounter in the three temperature regions.

Region I $C(T_o) < C_o < C_L(\text{eq}); \quad T_o < T < T_L(C_o);$

Point B below C_o

From the steady-state condition $C_o = C_s$ implies $C_s > C(T_o)$. As can be seen in Figures 3.2 and 1.8 steady-state solidification cannot occur in this region, because $\Delta G > 0$ for all possible values of C_L . Only non-steady-state solidification can occur in this region(20) with a solid composition in the allowed range of Figure 3.2, $C_s < C_o$. The rejection of solute enriches the liquid with a likely drop in solidification temperature or a breakdown of the plane front(34).

Region II $C_s(\text{eq}) < C_o < C(T_o); \quad T_s(C_o) < T < T_o;$

C_o lies between B and E

In this region steady-state solidification is possible provided that the composition of liquid remains in the range depicted in Figure 3.2. The solid formed is metastable with respect to partial remelting.

There is possible diffusional instability in such solidification as indicated by the down arrow in Figure 3.2. If momentarily the composition of the solid drops below C_0 , conservation of mass requires that the liquid be enriched in the minor component. Thus a downward fluctuation from the horizontal line ($C_s = C_0$) should result in a shift to the right (C_L increasing). If a system finds itself at a point F in the vicinity of E_{II} it cannot reestablish steady-state (climbing to the horizontal line) without decreasing C_L . But because the system is at F, the solid that is forming is below the average composition C_0 and the excess is rejected into the liquid making a reduction in C_L unlikely. Thus steady-state cannot be reestablished at this temperature and since we impose a velocity on the system the plane front interface again either breaks up or lags back to a lower temperature.

Steady-state solidification in region II is thus thermodynamically possible, but has difficulty in starting from equilibrium and could be diffusionaly unstable. It also leads to a metastable solid, which might in turn partially remelt.

Regardless of whether we have steady-state or not the solute experiences an increase in chemical potential upon solidification when $C_s > C_s(\text{eq})$ and solute trapping occurs. As we shall see in Chapter IV, this type of solidification is prohibited by various theories. The experimental finding of Zn-Cd in Chapter II indicates that solidification when $C_s > C_s(\text{eq})$ does occur.

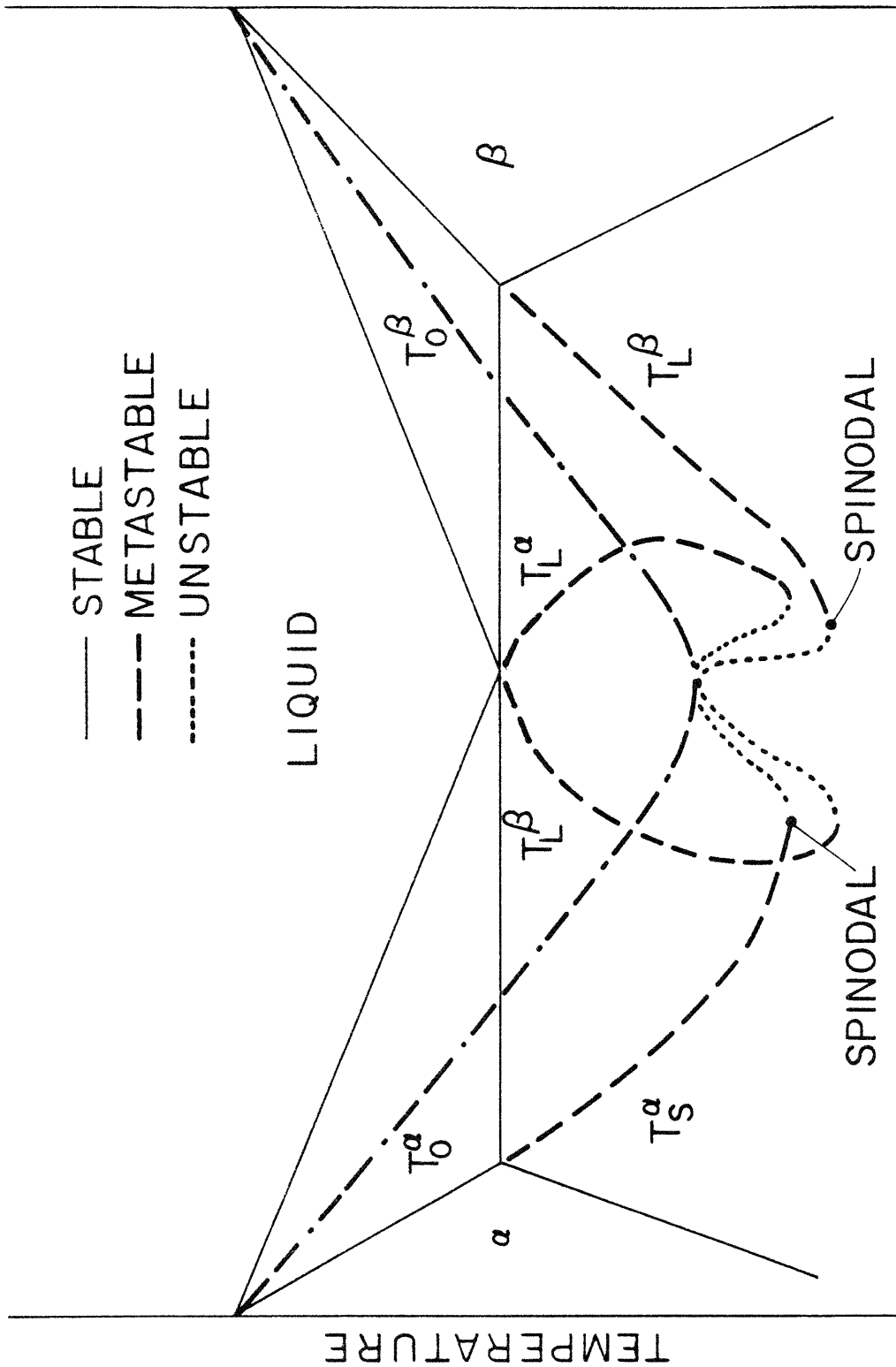
Region III $C_o < C_s(\text{eq}); T < T_s; C_o$ lies below E

Like region II steady-state growth of the solid is thermodynamically possible in this region. But unlike region II the resulting solid is stable. In addition the diffusional problem appears to be stable(22). If the system starts at point E_{III} , C_s will be greater than C_o and the liquid will be depleted of excess solute. Thus the system spontaneously leaves the point E_{III} and will settle somewhere on the horizontal line $C_s = C_o$ in Figure 3.2 for steady-state solidification.

Solute trapping occurs to the left of the intersection of line C_o with line OE. The diffusionless transformation (line OB) requires solute trapping and hence is not predicted by theories that forbid solute trapping. To the right of line OE no solute trapping is required, but to the right of PE solvent trapping begins. The equilibrium liquid concentration lies outside the

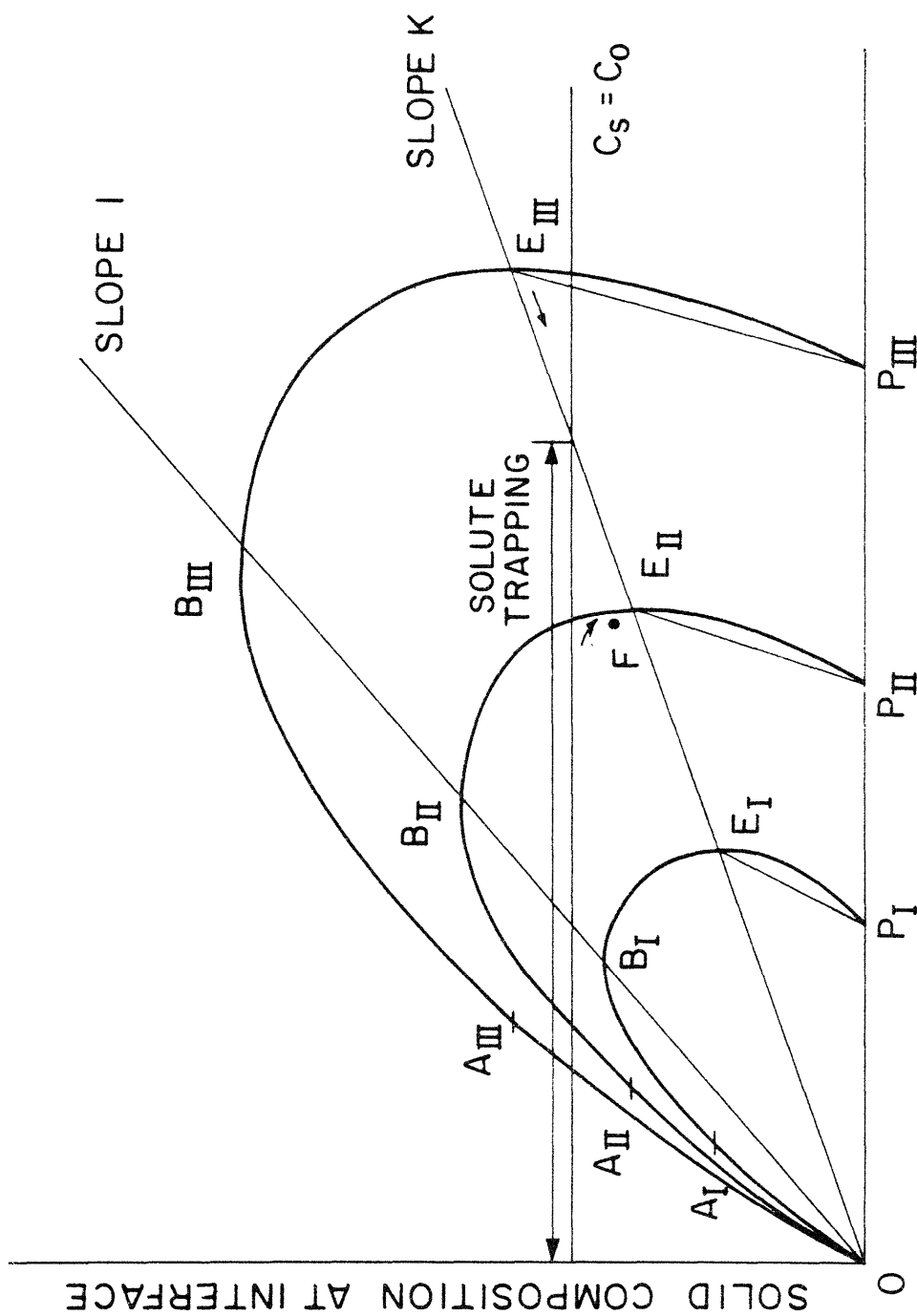
domain of the possible compositions in all regions except when $T = T_s$.

Local equilibrium. When the velocity V is very small but finite we must come close to the condition of local equilibrium. This means $T \sim T_s$ and the system is close to the point E . It is important to point out that the immediate vicinity of the point E could place the system either in region II or in region III. Conditions of solute trapping, solvent trapping, or no trapping at all are also infinitesimally close to the point E . Therefore one cannot argue a priori that because the system must approach E at low velocities that it comes to rest in any of these domains.



MOLE FRACTION B

Figure III-1. When there is a spinodal in the miscibility gap the stable-metastable phase diagram lines end when the solidus meets the spinodal. Further extensions of the metastable liquidus and solidus lines are unstable and intersect at a point on the T_0 line.



LIQUID COMPOSITION AT INTERFACE

Figure III-2. The domain of possible liquid interface compositions for steady-state solidification of an alloy of composition C_0 at three different temperatures. At steady-state C_s equals C_0 . As indicated by the arrows upward fluctuations in solid composition reduces the solute content of the liquid and downward fluctuations increase it. Steady-state can not be established by a system at point F in temperature region II. Local equilibrium can not be maintained in region III.

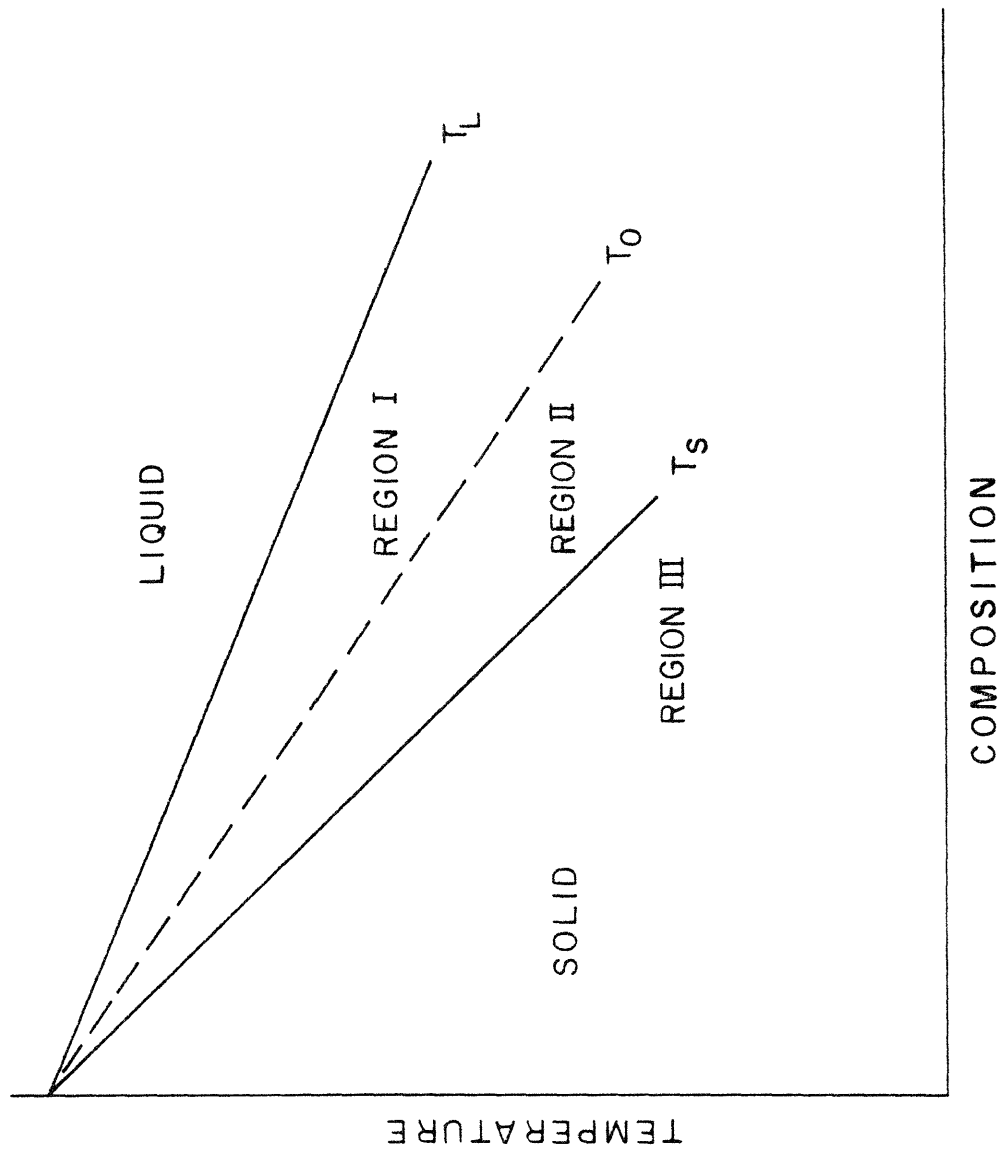


Figure III-3. Liquidus, solidus and T_O curves defining the three regions of temperature of figure III-2.

Chapter IV

IRREVERSIBLE THERMODYNAMICS OF INTERFACE PROCESSES

IV.1 Introduction

In this chapter we will describe methods of applying irreversible thermodynamics to interface processes during solidification and obtaining the interface response functions. The means of choosing the fluxes and thermodynamic forces for the various interface reactions will be examined. Four current theories using this approach will then be analyzed and compared with existing experimental results. Special attention will be focused on the following most often used assumptions and principles: the assumptions of independent reactions at the interface (no coupling of processes), the Onsager reciprocal relationships, and the principle of minimum entropy production. The section will be concluded by summarizing what has been learned about the validity of various aspects of the irreversible thermodynamic theories and where the field now stands.

IV.2 General Principles

The heart of irreversible thermodynamics (35,36,37) is that it proposes much needed relationships between rates of reactions and thermodynamic quantities. When applying it to the interface processes during

non-equilibrium solidification, the usual assumption is that the fluxes, J_i , across the interface and the conjugate thermodynamic forces, X_j are related linearly. In other words a phenomenological relation of the form

$$J_i = \sum_j L_{ij} X_j \quad (4.1)$$

is assumed for the interface reactions. The kinetic coefficients, L_{ij} , are phenomenological quantities to be determined for any given temperature. If there are only two processes occurring at the interface then equation (4.1) becomes

$$\begin{aligned} J_1 &= L_{11}X_1 + L_{12}X_2 \\ J_2 &= L_{21}X_1 + L_{22}X_2 \end{aligned} \quad (4.2)$$

In equation (4.2) the coefficients L_{11} and L_{22} relate each flux to its conjugate force. The cross coefficients, L_{12} and L_{21} , give the coupling interaction of the two processes. If the processes are independent, L_{12} and L_{21} are zero and

$$\begin{aligned} J_1 &= L_{11}X_1 \\ J_2 &= L_{22}X_2 \end{aligned} \quad (4.3)$$

There is, as we shall see, considerable freedom about the choice one may make for the independent fluxes and forces. Generally each flux-force pair is chosen such that

its product is a separate term satisfying the entropy production relationship(38)

$$T\sigma = J_1X_1 + J_2X_2 \quad (4.4)$$

where σ is the rate of entropy production. For example, a proper choice of flux-force pairs should not lead to a cross-term J_1X_2 . Because $T\sigma$ cannot be negative, if we define our flux-force pairs to satisfy equation (4.4), then the L matrix of equation (4.2) is required by thermodynamics to be positive definite(39) (or positive indefinite if there are infinitely large kinetic barriers to some of the reactions). This is

$$\begin{aligned} L_{11} &\geq 0 \\ L_{22} &\geq 0 \\ L_{12}L_{21} &\leq L_{11}L_{22} \end{aligned} \quad (4.5)$$

For isothermal processes $T\sigma = -dG/dt$ and for binary solidification at steady state

$$T\sigma = -\rho V [C_s \Delta\mu^B + (1 - C_s) \Delta\mu^A] \quad (4.6)$$

We will define two sets of flux-force pairs that satisfy equation (4.4) for the interface process in binary systems. Either of these are therefore equally valid variables for developing a theory of irreversible interface processes. Both have been used with some modification.

We can choose the J 's to be the net fluxes across the interface of the two species during steady-state growth

$$\begin{aligned} J_1' &= J^A = \rho V(1 - C_S) \\ J_2' &= J^B = \rho V C_S \end{aligned} \quad (4.7)$$

and the forces to be the chemical potential changes across the interface

$$\begin{aligned} X_1' &= -\Delta\mu^A \\ X_2' &= -\Delta\mu^B \end{aligned} \quad (4.8)$$

where $\Delta\mu^i = (\mu_S^i - \mu_L^i)$. Alternatively we might choose J_1 to be a total solidification flux without regard to composition change and J_2 to be what has been called a redistribution flux

$$\begin{aligned} J_1'' &= \rho V \\ J_2'' &= \rho V(C_S - C_L) \end{aligned} \quad (4.9)$$

Then we must choose

$$\begin{aligned} X_1'' &= -(1 - C_L) \Delta\mu^A - C_L \Delta\mu^B \\ X_2'' &= \Delta\mu^A - \Delta\mu^B \end{aligned} \quad (4.10)$$

X_1'' is the free energy change if components of the liquid add to the solid in the ratio in which they are in the liquid at the interface. It might be considered a driving force averaged according to the interface composition of

the liquid. The first reaction by itself ($J_2'' = 0$) would lead to solidification without a composition change. X_2'' is the driving force for the composition change across the interface. Together J_1'' and J_2'' describe any solidification reaction.

The reader may verify that both sets satisfy equation (4.4) algebraically. For the single primed set it is easily demonstrated graphically as well. For the double primed set, Figure 4.1 shows how the molar free energy change is apportioned among the flux-force pairs. ΔG_I is the free energy change due to the interface process when a mole solidifies at steady-state. ΔG_S is the free energy change due to the first flux-force pair and the difference in the slopes of the tangents times the composition difference is the free energy change due to the second flux-force pair.

Two ways of finding the independent processes have been given and for each process the proper driving force has been found. In the first set the fluxes of each species is tied to the thermodynamic driving force for that species. In the second the overall solidification rate is tied to an overall driving force which is the average of the driving force experienced by the atoms in the liquid, and the extent of redistribution is tied to the driving forces between the species. Either set is as complete as the other. They both give identical free energy changes.

A well-known condition in irreversible thermodynamics is the Onsager reciprocal relationships(40). It states

that $L_{12} = L_{21}$. We invite the reader to assume the relationship holds true in one of the primed sets and then substitute into the other set. It is immediately apparent that the Onsager relationship does not hold in the other set. It is often stated(41) that if the flux-force pairs are chosen to satisfy equation (4.4), the Onsager relationships are automatically guaranteed. This has been criticized(42) and the present example shows that this criticism is valid. The contradiction the reader will have found proves the Onsager relationships are not guaranteed by choosing our flux-force pairs to satisfy equation (4.4).

It is also tempting to assume that the fluxes are independent and set $L_{12} = L_{21} = 0$. However, in the examples above it is sobering to consider that if we make this assumption when using one set of flux-force pairs, the independence does not hold in the other set. For example if we assume

$$\begin{aligned} J_1' &= L_{11}'X_1' \\ J_2' &= L_{22}'X_2' \end{aligned} \tag{4.11}$$

then

$$\begin{aligned} X_1'' &= (1 - C_L)X_1' + C_L X_2' \\ X_2'' &= X_2' - X_1' \end{aligned} \tag{4.12}$$

Or solving for X's,

$$\begin{aligned} X_1' &= X_1'' - C_L X_2'' \\ X_2' &= X_1' + (1 - C_L)X_2'' \end{aligned} \tag{4.13}$$

And substitution leads to

$$J_1'' = J_1' + J_2' = [L'_{11} + L'_{22}] X_1'' + [-C_L L'_{11} + (1-C_L) L'_{22}] X_2'' \quad (4.14)$$

$$J_2'' = (C_S - C_L) J_1'' = (C_L - C_S) (L'_{11} + L'_{22}) X_1'' + (C_L - C_S) (-C_L L'_{11} + [1 - C_L] L'_{22}) X_2''$$

Now not only would these fluxes be coupled, but the off-diagonal terms are comparable to the diagonal. If

$$L''_{12} = 0 \text{ implies } L''_{22} = 0,$$

and

$$L''_{21} = 0 \text{ implies either } L''_{11} = 0 \\ \text{or } L''_{22} = 0.$$

In addition we note that again

$$L''_{12} \neq L''_{21} .$$

What this proves is that if the first set of flux-force pairs are assumed independent, the second set cannot be, and must appear coupled. We cannot assert a priori that because the flux-force pairs are chosen from equation (4.4) that they are uncoupled. Even though there is no contribution from $J_1 X_2$ or $J_2 X_1$ to $T\sigma$ we have no guarantee that there is not a contribution to J_1 from X_2 or vice versa. In fact the example shows the coupling can be quite large in one set when it was assumed absent in the other. Thus a perfectly simple flux-force relationship becomes very complicated when expressed in terms of another flux-force pair. It must be stressed that in going from the primed set to the double primed set no new physical

assumptions were made. The two sets of equations express the same physical behavior in different but compatible language, in that any experimental outcome can equally well be described in either set. The errors are introduced when someone makes a theoretical assertion about the L's.

Which of these two sets of flux-force pairs is the correct choice is not at issue. Both are capable of describing the same phenomenon. Of importance however is if we wish to assume that coupling between fluxes is weak and set cross terms equal to zero we must be careful. Compatibility with equation (4.4) is not a sufficient condition to insure the chosen fluxes and forces are independent, and does not guarantee that the Onsager's Reciprocal Relations ($L_{12} = L_{21}$) hold for the coupling terms.

Another principle that is commonly invoked is that at steady-state there is minimum entropy production (43,44,45). This can be used as a principle for obtaining relations among the L's but has often been criticized (42,46) on theoretical grounds as invalid. We shall show below that it leads to a result that contradicts solidification experiments.

Quite apart from these considerations, the assumption of linearity may not be valid when applied to the interface response. Several mechanisms of solidification, nucleation and lateral growth of new layers, and the spiral dislocation ramp would not lead to linear laws.

IV.3 Solidification Theories

The four irreversible thermodynamic theories to be discussed now are by Borisov(47), Baralis(43), Aptekar-Kamenetskaya(48), and Jindal-Tiller(49). The theories differ in the way the flux-force pairs are chosen. Another theory by Jackson(23) is of interest and will be discussed although it is not an irreversible thermodynamic theory. With minor differences the first two theories use the primed flux-force set, while the second two use the double primed set. Since additional assumptions are made about the L's, it is apparent the validity for both groups of theories is questionable. We will now consider the theories individually.

1. Borisov Theory

Borisov assumes the net fluxes of each atomic species traversing the interface is independent

$$\begin{aligned} J_A &= L_{AA} X_A \\ J_B &= L_{BB} X_B \end{aligned} \tag{4.15}$$

Since the above flux-force set is the primed set mentioned previously

$$\begin{aligned} J_A &= \rho V(1 - C_O) = \tau L_{AA} (\mu_S^A - \mu_L^A) \\ J_B &= \rho V C_O = \tau L_{BB} (\mu_S^B - \mu_L^B) \end{aligned} \tag{4.16}$$

By equations (4.5) L_{AA} and L_{BB} are always positive quantities. And since $\rho V(1 - C_0)$ and $\rho V C_0$ are positive for solidification, Borisov's theory yields the following condition:

$$\begin{aligned} \mu_s^A - \mu_L^A &< 0 \\ \mu_s^B - \mu_L^B &< 0 \end{aligned} \quad (4.17)$$

This limits the allowed processes to the triangle OEP of Figure 1.7 and implies no trapping of either atomic species is possible during solidification. For uncoupled reactions each species must traverse the interface only when it is thermodynamically favorable. This prediction is contrary to the Zn-Cd experimental result of solute trapping in Chapter II.

2. Jackson Theory

Unlike the other four theories, the Jackson theory is not an irreversible thermodynamic theory, but a kinetic description of alloy solidification. It is of interest since his resulting relationships have been put into the thermodynamic language of Borisov's. When doing so, the theory is seen to be equivalent to Borisov's (50). Jackson develops the theory on the basis of two assumptions:

(i) reaction rate theory can be applied independently for each species during solidification to determine the net flux of each type of atomic species across the interface, and (ii) the rate at which each atomic species leave a phase *and*

IV.3 Solidification Theories

The four irreversible thermodynamic theories to be discussed now are by Borisov(47), Baralis(43), Aptekar-Kamenetskaya(48), and Jindal-Tiller(49). The theories differ in the way the flux-force pairs are chosen. Another theory by Jackson(23) is of interest and will be discussed although it is not an irreversible thermodynamic theory. With minor differences the first two theories use the primed flux-force set, while the second two use the double primed set. Since additional assumptions are made about the L's, it is apparent the validity for both groups of theories is questionable. We will now consider the theories individually.

1. Borisov Theory

Borisov assumes the net fluxes of each atomic species traversing the interface is independent

$$\begin{aligned} J_A &= L_{AA} X_A \\ J_B &= L_{BB} X_B \end{aligned} \tag{4.15}$$

Since the above flux-force set is the primed set mentioned previously

$$\begin{aligned} J_A &= \rho V (1 - C_O) = -L_{AA} (\mu_S^A - \mu_L^A) \\ J_B &= \rho V C_O = -L_{BB} (\mu_S^B - \mu_L^B) \end{aligned} \tag{4.16}$$

traverse the interface is proportional to the mole fraction of the species in that phase. Assumption (i) necessarily leads to equation (4.17) and limits the theory to the triangle OEP of Figure 1.7.

3. Baralis Theory

Like Borisov, Baralis assumes the primed flux-force pairs, but he doesn't assume independent fluxes; i.e.,

$$J_A = \rho V(1 - C_O) = -L_{AA}(\mu_S^A - \mu_L^A) - L_{AB}(\mu_S^B - \mu_L^B) \quad (4.18)$$

$$\text{and } J_B = \rho VC_O = -L_{BA}(\mu_S^A - \mu_L^A) - L_{BB}(\mu_S^B - \mu_L^B).$$

Equations (4.18) are general and allow for coupling, which in turn permits the possibility of one of the species chemical potentials to increase upon solidification.

He assumes Onsager's Relationship, $L_{AB} = L_{BA}$, for the coupling coefficients. In addition he assumes that the rate of entropy production is a minimum for steady-state growth. In applying the latter assumption he arrives at the conclusion that

$$\mu_S^A - \mu_L^A < 0$$

$$\mu_S^B - \mu_L^B < 0$$

Hence, this analysis also limits the processes to the triangle OEP of Figure 1.7 and is contradicted by the Cd-Zn experiment. Even though the theory allows for

interaction of the two atomic-fluxes the principle of "minimum entropy production" restricts the coupling and forbids the possibility of trapping.

4. Aptekar-Kamenetskaya Theory

The interface processes assumed in this theory are equivalent to the double primed flux-force set, that is a total solidification reaction and redistribution reaction which are independent. The total solidification flux-force relationship is of a slightly different form, though, than for the double primed set, because of the dissimilarity in other assumptions. This treatment does not assume steady-state growth, but assumes the diffusivities in the liquid and solid phases are infinite (this implies the unlikely circumstance of the two phases having uniform composition at any instant of time). The above condition for most growth rates leads to a variation of liquid and solid compositions at the interface with solidification time, which in turn corresponds to a driving force across the interface that is a function of time. As a result, there is a subtle distinction between the two expressions of driving force for the total solidification reaction. It also should be added that this treatment is not a complete theory since the number of unknown quantities exceeds the number of equations. Regardless of the above serious shortcomings, Aptekar and Kamenetskaya do predict the possibility of solute trapping, $\mu_S^B - \mu_L^B > 0$.

5. Jindal-Tiller Theory

In principle, this theory also assumes the double primed set, although the only reactions considered in detail are the redistribution reactions

$$J_R^B = \rho V (C_S - C_L) = -L_R^B (\mu_S^B - \mu_L^B) \quad (4.19)$$

$$J_R^A = \rho V (C_L - C_S) = -L_R^A (\mu_S^A - \mu_L^A) \quad (4.20)$$

If L_R^B and L_R^A are chosen to be the interdiffusion kinetic coefficients, then $L_R^B = L_R^A$ and combining equations (4.19) and (4.20) yield the double primed redistribution relation

$$J_R = \rho V (C_S - C_L) = L_R (\Delta\mu_A - \Delta\mu_B) \quad (4.21)$$

where $L_R = L_R^B/2$. Comparison of equations (4.19) and (4.20) shows that $\Delta\mu_A$ and $\Delta\mu_B$ always have opposite signs. Thus this theory restricts the process to lie outside the triangle OEP but inside the curve OABEP where trapping always occurs.

It should be noted that the expression for the total solidification flux-force pair should be solved simultaneously with equations (4.19) and (4.20), otherwise the various values of the growth rate V may be unrealistic. Also it is not certain that equation (4.4) is satisfied since no expression for the total solidification reaction was given. A major deficiency of this theory is that C_S/C_L does not equal $K(\text{eq})$

when $V = 0$, but $(2\sqrt{K(\text{eq})} - 1)$. (See their Figure 6.)

A limiting condition for all correct theories should be

$$C_S/C_L = K(\text{eq}) \text{ when } V = 0.$$

IV.4 Discussion of Theories

It has been shown earlier from classical thermodynamics that for solidification the compositions of the solid and liquid at the interface must be inside the OABEP curve of Figure 1.7. In this section it has been shown that irreversible thermodynamics is unreliable in attempts to restrict the two compositions further. Theories using similar assumptions can arrive at contrary results. For example, Borisov assumes his flux-force pairs are uncoupled and finds trapping to be impossible, where as Jindal and Tiller make the same assumption for their flux-force pairs and find trapping always occurs. The basic difference in the two approaches is that they choose different coordinate systems for the atomic fluxes, J_A and J_B , which are proportional to $\Delta\mu_A$ and $\Delta\mu_B$. Borisov uses the one moving with the interface which gives a constant flux of material for steady-state for the minor component

$$J_B = V\rho C_S,$$

while Jindal and Tiller chooses a substantial or laboratory coordinate system imbedded in the liquid which differs by

$$V\rho C_L$$

$$J_B = V\rho(C_S - C_L)$$

For the usual case where $C_L > C_S$ the two J_B 's have opposite signs and, if uncoupled, lead to opposite signs in $\Delta\mu^B$.

We should also point out that all four irreversible thermodynamic theories have serious deficiencies. New principles are required in this field or tighter restrictions for applying the old principles are necessary. But most of all, there is a need for experiments to study the deviations from local equilibrium and coupling effects.

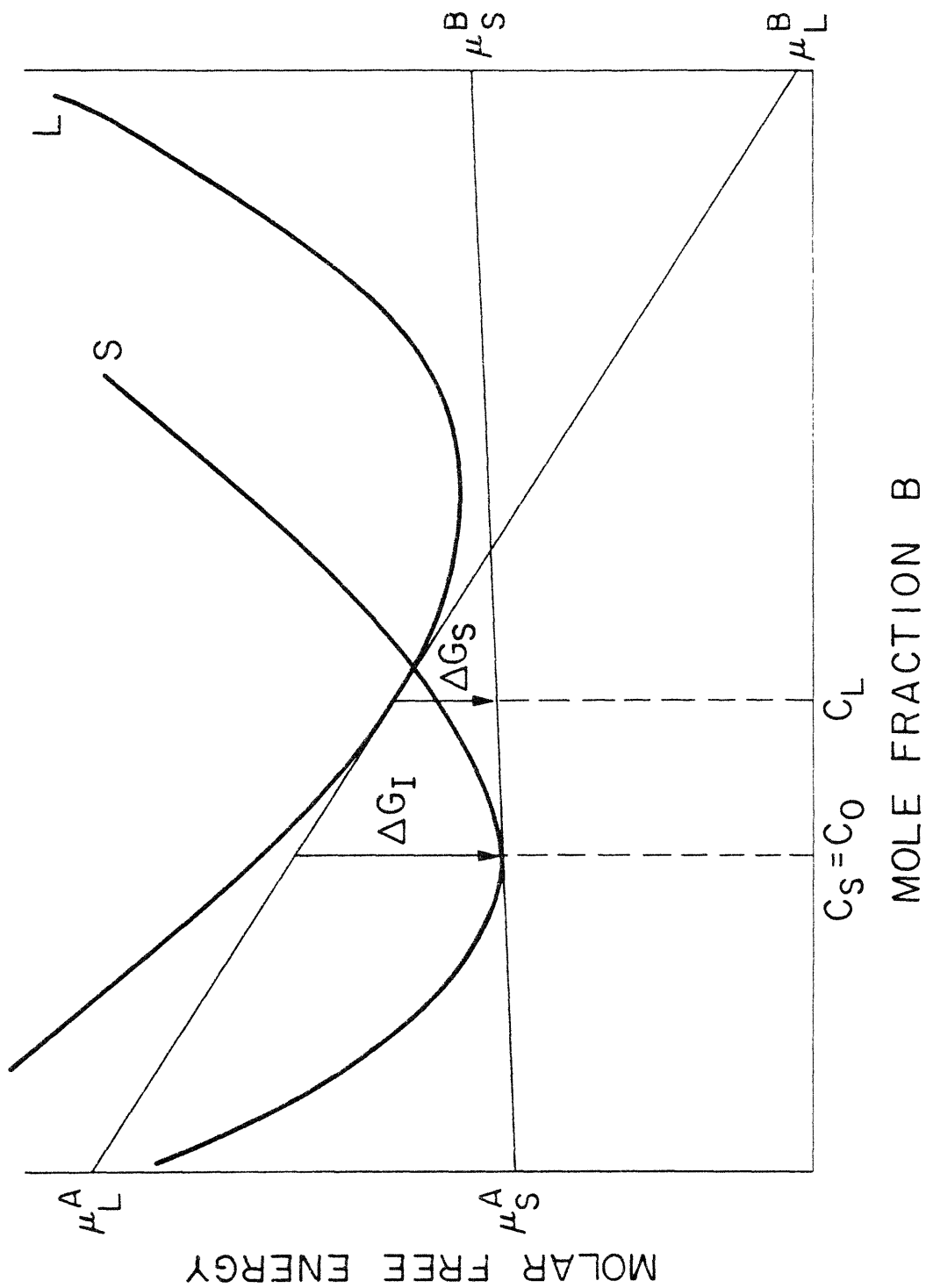


Figure IV-1. In the double primed set the free energy change per mole of solid formed ΔG_I is apportioned among a solidification reaction Δ for which the driving force is $\Delta\mu$ averaged among the atoms in the liquid at the interface and a redistribution in which the differences in $\Delta\mu$ act to bring about the composition difference $(C_L - C_0)$.

Chapter V

AN ALTERNATE APPROACH TO INTERFACE PARTITIONING DURING SOLIDIFICATION

V.1 Introduction

In the previous chapter it was found that the method of irreversible thermodynamics as applied to the study of interface processes during solidification leads to values of interface distribution coefficients that were questionable. The present chapter is devoted to overcoming this shortcoming by using a different approach to the problem. The method of Solute Interface Drag will be applied. Specifically, an attempt to solve for the liquid and solid interface compositions for an imposed and specified velocity is made when the moving interface is represented by a potential well in motion. It is assumed in regard to the solute species, that the interface at a given temperature can be characterized by a solute interaction energy $E(x)$ and a diffusion coefficient $D(x)$. Both $E(x)$ and $D(x)$ are functions of an arbitrarily chosen plane in the interface.

V.2 Diffusional Solution

Let us assume dilute solution everywhere, then the chemical potential of the solute species is given by equation (I.5)

$$\mu = kT \ln C(x) + E(x) + \text{constant} \quad (5.1)$$

where E for the liquid and solid are related by

$$(E_L - E_S) = kT \ln \frac{C_S(\text{eq})}{C_L(\text{eq})} \quad (5.2)$$

Now define the interdiffusion coefficient as

$$D(x) = - JkT / \left(\frac{\partial \mu}{\partial x} \right) C \quad (5.3)$$

where J is the flow of atoms per cm^2 per sec. measured in a co-ordinate system fixed in the liquid phase. Volume changes are neglected. Combining equations (5.1) and (5.3) the flux becomes

$$-J = \frac{DC}{kT} \frac{\partial \mu}{\partial x} = D \frac{\partial C}{\partial x} + \frac{DC}{kT} \frac{\partial E}{\partial x} \quad (5.4)$$

The first term on the right-hand side of this equation is the well known fickian flux, and the second term is the flux resulting from the interfacial potential gradient $\partial E / \partial x$. However, a fixed co-ordinate system relative to the interface is mathematically desired and for this new co-ordinate system the flux relationship becomes

$$-J = D \frac{\partial C}{\partial x} + \frac{DC}{kT} \frac{\partial E}{\partial x} + VC \quad (5.5)$$

With regard to this new co-ordinate system, the conservation equation becomes

$$\frac{\partial C}{\partial t} = D \frac{\partial^2 C}{\partial x^2} + \left[V + \frac{\partial D}{\partial x} + \frac{D}{kT} \frac{\partial E}{\partial x} \right] \frac{\partial C}{\partial x} + \frac{C}{kT} \left[\frac{\partial D}{\partial x} \frac{\partial E}{\partial x} + D \frac{\partial^2 E}{\partial x^2} \right] \dots \dots \dots (5.6)$$

This relationship at any instant in time must be satisfied at each point in the system, the composition C being a function of both position x and time t . It has to be solved for given initial and boundary conditions.

Relative to the interface fixed co-ordinate system and under steady-state conditions, the composition everywhere remains unchanged with respect to time. Therefore $\partial C/\partial t = 0$ and $J = \text{constant}$, and equation (5.6) may be expressed as

$$0 = \frac{\partial}{\partial x} \left(-D \frac{\partial C}{\partial x} - \frac{DC}{kT} \frac{\partial E}{\partial x} - VC \right) = \frac{\partial}{\partial x} (J) \quad (5.8)$$

This is a necessary result for the satisfaction of steady-state conditions where J is a constant. Integration from $-\infty$ to x yields

$$0 = \int_{-\infty}^x \frac{\partial J}{\partial x} dx = \int_{-\infty}^x dJ = J(x) - J(-\infty) \quad (5.9)$$

or

$$0 = \left[-D \frac{\partial C}{\partial x} - \frac{DC}{kT} \frac{\partial E}{\partial x} - VC \right] + VC_0 \quad (5.10)$$

Rewriting the above equation

$$\frac{\partial C}{\partial x} + \left[\frac{1}{kT} \frac{\partial E}{\partial x} + \frac{V}{D} \right] C = \frac{V}{D} C_0 \quad (5.11)$$

It is readily seen that the above equation is a linear differential equation of the first order and can be solved in general terms without determining separately homogeneous

and particular solutions. The form of the equation is

$$\frac{\partial Y}{\partial x} + P(x)Y = Q(x) \quad (5.12)$$

which can be solved by using a standard integrating factor
(5.1)

$$\text{I.F.} = \exp\left[\int P(x) dx\right] \quad (5.13)$$

The solution of equations of the form (5.12) is obtained by the following integration:

$$Y = \frac{1}{(\text{I.F.})} \int_{x=-\infty}^{x=x} (\text{I.F.}) Q(x) dx \quad (5.14)$$

Hence, the solution of equation (5.11) becomes

$$C(x) = VC_0 \exp\left\{-\frac{E(x)}{kT} - v \int_{x_0}^x \frac{dn}{D(n)}\right\} \cdot \int_{-\infty}^x \exp\left[\frac{E(\xi)}{kT} + v \int_{x_0}^{\xi} \frac{dn}{D(n)}\right] \frac{d\xi}{D(\xi)} \quad \dots (5.15)$$

The above relationship is the exact solution to equation (5.11), and is completely general as long as the assumptions in equations (5.1) and (5.3) hold. It describes the composition everywhere for any imposed velocity at steady-state for arbitrary $E(x)$ and $D(x)$. The limiting conditions of equation (5.15) are difficult to determine. But it can be easily shown from equation (5.1) that the ratio of the interface compositions of the solid and liquid is given by

$$\frac{C_s(i)}{C_L(i)} = \exp\left(\frac{E_s - E_L}{kT}\right) = K(\text{eq}) \quad (5.16)$$

when $V = 0$. This is a necessary limiting condition for any valid theory. Later in the section it will be shown that equation (5.15) reduces to condition (5.16) when $V = 0$ and to another limiting condition

$$\frac{C_s(i)}{C_L(i)} \rightarrow 1 \quad (5.17)$$

when $V \rightarrow \infty$

V.3 Graphical Representation

As pointed out above, equation (5.15) describes the composition profile at steady-state for an arbitrary $E(x)$ and $D(x)$. This relationship then not only yields the desired interface compositions but also the compositions everywhere else. Nevertheless this section will focus only on understanding the nature of the interface partitioning. To represent graphically some of the properties of equation (5.15), $D(x)$ and $E(x)$ are assumed to be functions of x as shown in Figure 5.1. For such a model, equation (5.15) can be reduced to yield the following expression for the interface partitioning:

$$\begin{aligned} \frac{C_L(i)}{C_s(i)} &= \frac{C_L(i)}{C_o} = \exp\left(\frac{E_S - E_L}{kT}\right) \left\{ \exp\left(\frac{-\delta V}{D_s}\right) \exp\left(\frac{-\delta V}{D_L}\right) + \right. \\ &\left[\frac{1}{1 + \frac{D_s}{\delta V} \left(\frac{E_B - E_S}{kT}\right)} \right] \left[\exp\left(\frac{-\delta V}{D_L}\right) \left[\exp\left(\frac{E_B - E_S}{kT}\right) - \exp\left(\frac{-\delta V}{D_s}\right) \right] + \right. \\ &\left. \left[\frac{1}{1 + \left(\frac{D_L}{\delta V}\right) \left(\frac{E_L - E_B}{kT}\right)} \right] \left[\exp\left(\frac{E_L - E_S}{kT}\right) \right] \left[1 - \exp\left(\frac{E_B - E_L}{kT}\right) \exp\left(\frac{-\delta V}{D_L}\right) \right] \right\} \\ &\dots\dots (5.18) \end{aligned}$$

as shown in the appendix. In terms of the equilibrium distribution coefficient, $K(\text{eq})$, equation (5.18) becomes

$$\frac{C_L(i)}{C_S(i)} = \frac{C_L(i)}{C_O} = \frac{1}{K(\text{eq})} [e^{-X-Y} + \left(\frac{1}{\ln \frac{K(\text{eq})}{K_B(\text{eq})}} \right) (e^{-Y}) \left(\frac{K(\text{eq})}{K_B(\text{eq})} - e^{-X} \right) + \left(\frac{1}{\ln \frac{K(\text{eq})}{K_B(\text{eq})}} \right) (K(\text{eq})) \left(1 - \frac{e^{-Y}}{K_B(\text{eq})} \right)] \quad (5.19)$$

where $K_B(\text{eq})$, X , and Y are defined as in the appendix. For the case where $K(\text{eq})$ is a constant this kinetic result (equation 5.19) is only dependent on the imposed velocity and not on the interface temperatures.

The graphical representation of equation (5.19) for a typical $K(\text{eq}) = 10^{-1}$ is given in Figure 5.2. The various curves are for different assumed values of $K_B(\text{eq})$ or $(E_L - E_B)$. Curves 1 and 2 show the nature of the dependence of the interface partitioning on the growth velocity when the solute species is surface desorbed at equilibrium. Curves 5 and 6 are for the case when the solute species is surface active (surface adsorption at equilibrium). Curves 3 and 4 show the partition when the equilibrium interface composition is equal to the equilibrium solid and liquid compositions.

Let us now consider in detail the case when the solute atoms are surface inactive (curves 1 and 2). The initial deviations from local equilibrium are negative, $K < K(\text{eq})$, that is for a given steady-state solid composition the liquid interface composition increases with growth velocity. Since

$E_B > E_L$ the solute species attempt to remain in the liquid and avoid the moving interface; this leads to an increase in the liquid interface composition as the velocity increases because the diffusion distances in the liquid relative to the interface per unit time are decreasing with increasing interface velocity. One can then conclude since $K < K(eq)$, the solidification must take place when C_S and T lie in the single-phase solid region on the equilibrium phase diagram to allow $C_L(i) < C_L(eq)$ which is a thermodynamic requirement.

At higher growth velocities we see curves 1 and 2 pass through a maximum and then $\log (C_L(i)/C_S)$ converges continuously to zero. The reason for this behavior is that the solute species has increasing difficulty remaining in the liquid by diffusing ahead of the interface at these higher steady state velocities. When $\log (C_L(i)/C_S)$ becomes zero the transformation may be considered as diffusionless. From the above reasoning one can conclude that if the diffusivity in the liquid were larger than for the case in Figure 5.2, the maximum in curves 1 and 2 would be shifted to a larger velocity. The same is true for the velocity needed for a diffusionless transition.

It is also of interest to analyze curves 1 and 2 in terms of solute trapping, $K > K(eq)$. From Figure 5.2 it is necessary for $\log Y > 0$ for solute trapping to occur, or $V > 10^2$ cm/sec. Such large velocities may be physically

unrealistic and hence solute trapping is most likely impossible when $E_B > E_L$.

Turning now to the case where the solute atoms are surface active, $E_B < E_L$ and curves 5 and 6, it is observed that any deviation from local equilibrium is positive. Hence solidification in the two phased region, $C_S > C_S(\text{eq})$, is possible and solute trapping will always result no matter in what region of the phase diagram the solidification occurs. This behavior is rationalized because during freezing the solute atoms rush to the interface from the liquid when $E_B < E_L$ and then are captured in solid such that $K > K(\text{eq})$ even though $E_B < E_S$. The reason for this is because the diffusivity of the interface is changing from D_L on the liquid side to a smaller value, D_S , on the solid side. Such a phenomena also allows it to be kinetically possible to have $C_S(i) > C_L(i)$ at large velocities, but which are smaller than those necessary for a diffusionless transformation.

Similar to the above, the intermediate cases, curves 3 and 4, result in positive departures from local equilibrium at high velocities because of the difference in diffusivity across the interface. But $C_S(i) > C_L(i)$ is not possible because the solute species does not rush to the interface as in the previous case. The solute species in the liquid is more or less not affected by the interface potential since $E_S \leq E_B \leq E_L$.

As noted in Section I.3 of the first chapter, the most plausible assumption concerning the nature of the interface is to assume it to be disordered and similar to the liquid phase. Then $E_B \approx E_L$ and the partitioning is represented by curve 4 of Figure 5.2. For this probable case solute trapping will always occur during steady-state solidification and $C_L(i)$ will monotonically decrease from $C_0/K(eq)$ to C_0 with increasing growth velocity. Curve 4 shows the condition of local equilibrium at the interface to be a good assumption for velocities of millimeters per second or smaller. The transformation becomes diffusionless with velocities larger than centimeters per second. It should be kept in mind that these estimates are for the particular model developed in the appendix.

V.4 Appendix

In this section equation (5.15) will be integrated for the case where $D(x)$ and $E(x)$ are assumed to be functions of x as shown in Figure 5.1. The origin of the x -axis is taken as the solid side of the interface. The center of the interface $x = \delta$ is where $E = E_B$. The liquid side of the interface is at $x = 2\delta$. The interdiffusion coefficient is assumed to change from D_S to D_L at $x = \delta$.

Equation (5.15) will be integrated from $-\infty$ to 2δ since the interface liquid composition is desired for determining the interface partitioning. Equation (5.15) is now rewritten.

$$C(x) = C_0 V \exp\left[-\frac{E(x)}{kT} - V \int_{x_0}^x \frac{dn}{D(n)}\right] \cdot \int_{-\infty}^x \exp\left(\frac{E(\xi)}{kT} + V \int_{x_0}^{\xi} \frac{dn}{D(n)}\right) \frac{d\xi}{D(\xi)} \quad (5.15)$$

The second integral in equation (5.15) is broken up into the sum of the following three integrals.

$$\text{INTEGRAL } \textcircled{1} = \int_{-\infty}^0 \exp\left[\frac{E(\xi)}{kT} + V \int_{x_0}^{\xi} \frac{dn}{D(n)}\right] \frac{d\xi}{D(\xi)}$$

$$\text{INTEGRAL } \textcircled{2} = \int_0^{\delta} \exp\left[\frac{E(\xi)}{kT} + V \int_{x_0}^{\xi} \frac{dn}{D(n)}\right] \frac{d\xi}{D(\xi)}$$

$$\text{INTEGRAL (3)} = \int_{\delta}^{2\delta} \exp \left[\frac{E(\xi)}{kT} + V \int_{x_0}^{\xi} \frac{dx}{D(x)} \right] \frac{d\xi}{D(\xi)}$$

$$x_0 \equiv 0$$

CONSIDERING INTEGRAL (1)

$$\text{INTEGRAL (1)} = \int_{-\infty}^0 \exp \left[\frac{E(\xi)}{kT} + V \int_{x_0}^{\xi} \frac{dx}{D(x)} \right] \frac{d\xi}{D(\xi)}$$

FROM FIGURE V-1

$$\begin{aligned} D &= D_s \\ E &= E_s \end{aligned} \quad \text{for } -\infty \leq \xi \leq 0$$

AND

$$V \int_0^{\xi} \frac{dx}{D(x)} = \frac{V}{D_s} \xi \quad \text{for } \xi < 0$$

REWRITING INTEGRAL (1)

$$\text{INTEGRAL (1)} = \frac{1}{D_s} \int_{-\infty}^0 \exp \left[\frac{E_s}{kT} + \frac{V}{D_s} \xi \right] d\xi$$

CHANGING VARIABLE OF INTEGRATION

$$du = \frac{V}{D_s} d\xi$$

$$\text{INTEGRAL (1)} = \int_{\xi=-\infty}^{\xi=0} \exp \left[\frac{E_s}{kT} + \frac{V}{D_s} \xi \right] du$$

$$\text{INTEGRAL (1)} = \frac{1}{V} \exp \frac{E_s}{kT} \quad (5.20)$$

TURNING NOW TO INTEGRAL (2)

$$\text{INTEGRAL (2)} = \int_0^{\delta} \exp \left[\frac{E(\xi)}{kT} + V \int_{x_0}^{\xi} \frac{dn}{D(\eta)} \right] \frac{d\xi}{D(\xi)}$$

FROM FIGURE V-1

$$D = D_s \quad \text{for } 0 \leq x \leq \delta$$

$$E = E_s - \frac{x}{\delta} (E_s - E_B)$$

$$\text{AND } V \int_0^{\xi} \frac{dn}{D(\eta)} = \frac{V}{D_s} \xi \quad \text{for } \xi < \delta$$

REWRITING INTEGRAL (2)

$$\text{INTEGRAL (2)} = \int_0^{\delta} \exp \left[\frac{E_s - \frac{\xi}{\delta} (E_s - E_B)}{kT} + \frac{V}{D_s} \xi \right] \frac{d\xi}{D_s}$$

$$\text{INTEGRAL (2)} = \int_0^{\delta} \exp \left[\frac{D_s E_s - \frac{\alpha}{\delta} (E_s - E_B) \xi + V k T \xi}{k T D_s} \right] \frac{d\xi}{D_s}$$

$$du = \left[\frac{V k T - \frac{D_s}{\delta} (E_s - E_B)}{k T D_s} \right] d\xi$$

$$\text{INTEGRAL (2)} = \frac{k T}{V k T - \frac{D_s}{\delta} (E_s - E_B)} \left[\exp \left(\frac{D_s E_s + [V k T - \frac{D_s}{\delta} (E_s - E_B)] \xi}{k T D_s} \right) \right]_0^{\delta}$$

THE FINAL EXPRESSION FOR INTEGRAL (2) IS :

$$\text{INTEGRAL (2)} = \left[\frac{k T \exp \left(\frac{E_s}{k T} \right)}{V k T + \frac{D_s}{\delta} (E_B - E_s)} \right] \left[\exp \left(\frac{(E_B - E_s)}{k T} + \frac{V \delta}{D_s} \right) - 1 \right] \quad (5.21)$$

NOW EVALUATING INTEGRAL (3)

$$\text{INTEGRAL (3)} = \int_{\delta}^{2\delta} \exp \left[\frac{E(\xi)}{k T} + V \int_{x_0}^{\xi} \frac{dn}{D(n)} \right] \frac{d\xi}{D(\xi)}$$

FROM FIGURE V-1

$$D = D_L \quad \text{for } \delta \leq \xi \leq 2\delta$$

$$E(\xi) = E_B + \frac{\xi - \delta}{\delta} (E_L - E_B)$$

$$\text{AND } V \int_{x_0=0}^{\xi} \frac{dn}{D(n)} = V \left[\frac{\delta}{D_s} + \frac{\xi - \delta}{D_L} \right] \quad \text{for } \xi > \delta$$

REWRITING INTEGRAL (3)

$$\text{INTEGRAL (3)} = \int_{\delta}^{2\delta} \exp \left[\frac{E_B + \frac{\xi - \delta}{\delta} (E_L - E_B)}{kT} + V \left(\frac{\delta}{D_s} + \frac{\xi - \delta}{D_L} \right) \right] d\xi$$

$$du = \left[\frac{\frac{D_L}{\delta} E_L - E_B + V k T}{k T V} \right] d\xi$$

$$\text{INTEGRAL (3)} = \left[\frac{kT}{\frac{D_L}{\delta} (E_L - E_B) + V k T} \right] \cdot \left[\exp \frac{E_B}{kT} + \frac{V\delta}{D_s} \right] \cdot$$

(5.22)

$$\left[\exp \left(\frac{E_L - E_B}{kT} + \frac{\delta V}{D_L} \right) - 1 \right]$$

REWRITING EQUATION (5.15) IN TERMS OF THE THREE INTEGRALS AND EVALUATED AT $(x=2\delta)$.

$$C'(2\delta) = C_0 V \exp \left[-\frac{E_L}{kT} - \frac{\delta V}{D_s} - \frac{\delta V}{D_L} \right] \left[\text{INT. (1)} + \text{INT. (2)} + \text{INT. (3)} \right]$$

DEFINE

$$Q \equiv C_0 V \exp \left[-\frac{E_L}{kT} - \frac{\delta V}{D_s} - \frac{\delta V}{D_L} \right] \quad (5.23)$$

Now

$$C(2\delta) = Q \left[I_{NT.①} + I_{NT.②} + I_{NT.③} \right]$$

FURTHER DEFINE

$$Q_1 \equiv Q \left[I_{NT.①} \right]$$

$$Q_2 \equiv Q \left[I_{NT.②} \right] \quad (5.24)$$

$$Q_3 \equiv Q \left[I_{NT.③} \right]$$

THEN

$$C(2\delta) = Q_1 + Q_2 + Q_3 \quad (5.25)$$

CONSIDER Q_1

COMBINING EQUATIONS (5.20), (5.23), & (5.24)

$$Q_1 = C_0 V \exp\left(-\frac{E_L}{kT} - \frac{\delta V}{D_S} - \frac{\delta V}{D_L}\right) \frac{1}{V} \exp\left(\frac{E_S}{kT}\right)$$

OR

$$Q_1 = C_0 \exp\left[\frac{E_S - E_L}{kT}\right] \exp\left[-\frac{\delta V}{D_S}\right] \exp\left[-\frac{\delta V}{D_L}\right] \quad (5.26)$$

CONSIDER Q_2

COMBINING EQUATIONS (5.21), (5.23), & (5.24)

$$Q_2 = C_0 \left[\frac{1}{1 + \left(\frac{D_s}{\delta V}\right) \frac{E_B - E_s}{kT}} \right] \exp \left[\frac{E_s - E_L}{kT} - \frac{\delta V}{D_s} - \frac{\delta V}{D_L} \right] \cdot \quad (5.27)$$

$$\left[\exp \left(\frac{E_B - E_s}{kT} + \frac{V\delta}{D_s} \right) - 1 \right]$$

CONSIDER Q_3

COMBINING EQUATIONS (5.22), (5.23) & (5.25)

$$Q_3 = C_0 \left[\frac{1}{1 + \left(\frac{D_L}{\delta V}\right) \frac{E_L - E_B}{kT}} \right] \left[1 - \exp \left(\frac{E_B - E_L}{kT} - \frac{\delta V}{D_L} \right) \right] \quad (5.28)$$

COMBINING EQUATIONS (5.25), (5.26), (5.27), & (5.28) WE OBTAIN EQUATION (5.18) OF THE PREVIOUS SECTION

$$\frac{C(2\delta)}{C_0} = \frac{C_L(i)}{C_s(i)} = \exp \left(\frac{E_s - E_L}{kT} \right) \left[\exp \left(-\frac{\delta V}{D_s} \right) \exp \left(-\frac{\delta V}{D_L} \right) + \right.$$

$$\left. \left[\frac{1}{1 + \left(\frac{D_s}{\delta V}\right) \frac{E_B - E_s}{kT}} \right] \left[\exp \left(-\frac{\delta V}{D_L} \right) \left[\exp \left(\frac{E_B - E_s}{kT} \right) - \exp \left(-\frac{V\delta}{D_s} \right) \right] + \right.$$

$$\left. \left[\frac{1}{1 + \left(\frac{D_L}{\delta V}\right) \frac{E_L - E_B}{kT}} \right] \left[\exp \left(\frac{E_L - E_s}{kT} \right) \left[1 - \exp \left(\frac{E_B - E_L}{kT} \right) \exp \left(-\frac{\delta V}{D_L} \right) \right] \right]$$

..... (5.18)

FOR CONVENIENCE EQUATION (5.18) CAN BE EXPRESSED IN TERMS OF THE FOLLOWING PARAMETERS :

$$K(\text{eq}) \equiv \exp\left(\frac{E_L - E_S}{KT}\right) = \frac{C_S(\text{eq})}{C_L(\text{eq})}$$

$$K_B(\text{eq}) \equiv \exp\left(\frac{E_L - E_B}{KT}\right) = \frac{C_B(\text{eq})}{C_L(\text{eq})}$$

$$X \equiv \frac{\delta'V}{D_S}$$

$$Y \equiv \frac{\delta'V}{D_L}$$

$\frac{C_L(i)}{C_S(i)}$ BECOMES

$$\frac{C_L(i)}{C_S(i)} = \frac{1}{K(\text{eq})} \left[\exp(-X-Y) + \left(\frac{1}{1 + \ln K(\text{eq})/K_B(\text{eq})} \right) \left(\frac{1}{X} \right) \exp(-Y) \right] \cdot \left(\frac{K(\text{eq})}{K_B(\text{eq})} - \exp(-X) \right) + \left(\frac{K(\text{eq})}{1 + \ln K_B(\text{eq})} \right) \left(\frac{1 - \exp(-Y)}{K_B(\text{eq})} \right) \quad (5.19)$$

THIS IS THE EQUATION PLOTTED IN FIGURE V-2. IT IS ASSUMED THAT $D_S = 10^{-3} D_L$. IN THE NOTATION OF THIS FIGURE $V \equiv R$, $K(\text{eq}) \equiv K$, AND $K_B(\text{eq}) = K_B$.

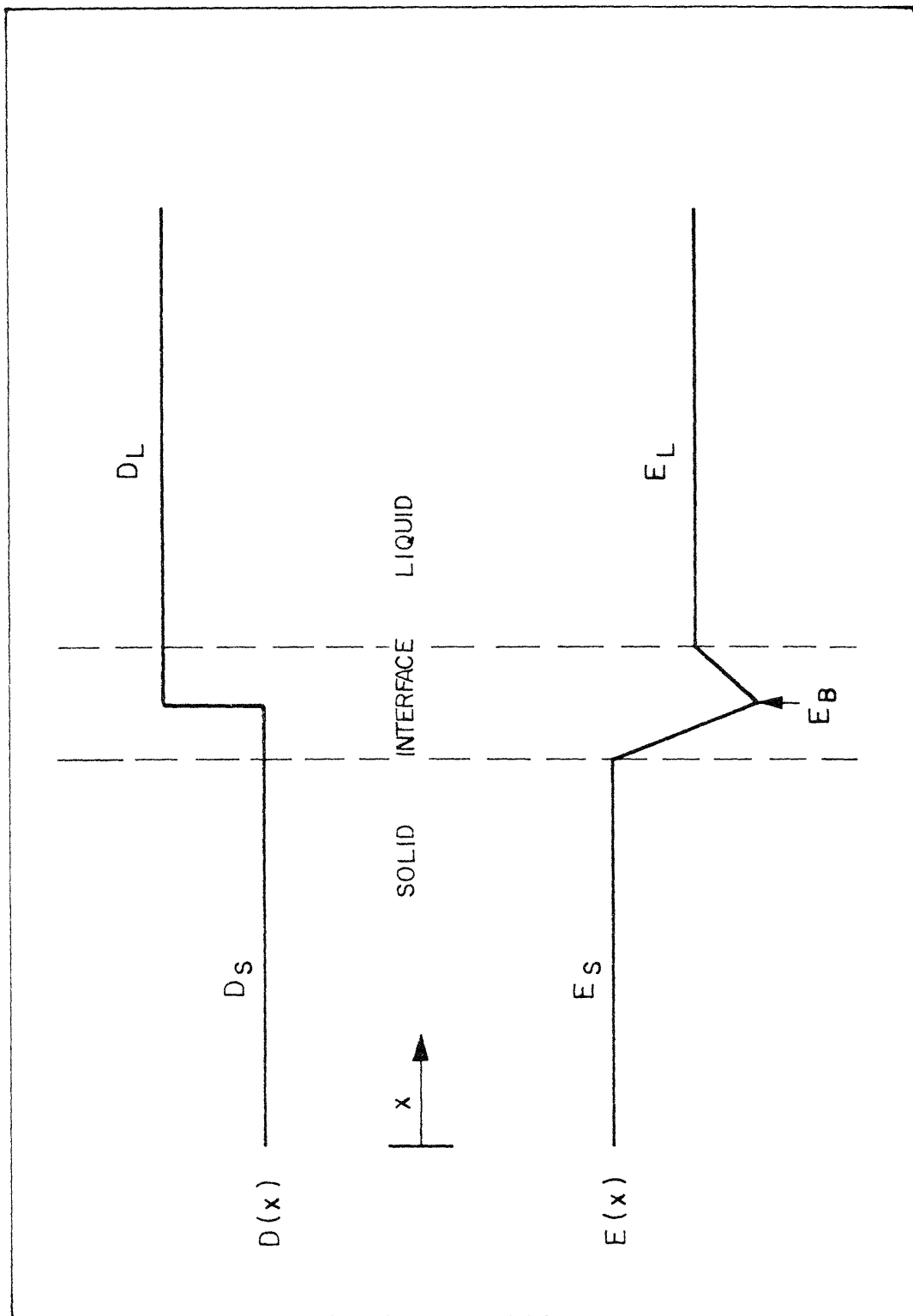


Figure V-1. Graphical illustration of the interdiffusion coefficient $D(x)$ and the solute interaction energy $E(x)$ as a function of distance x through the interface. The value of the solute interaction energy at the center of the boundary E_B will be allowed to vary from $E_B \ll E_L$ to $E_B \gg E_S$ in the analysis

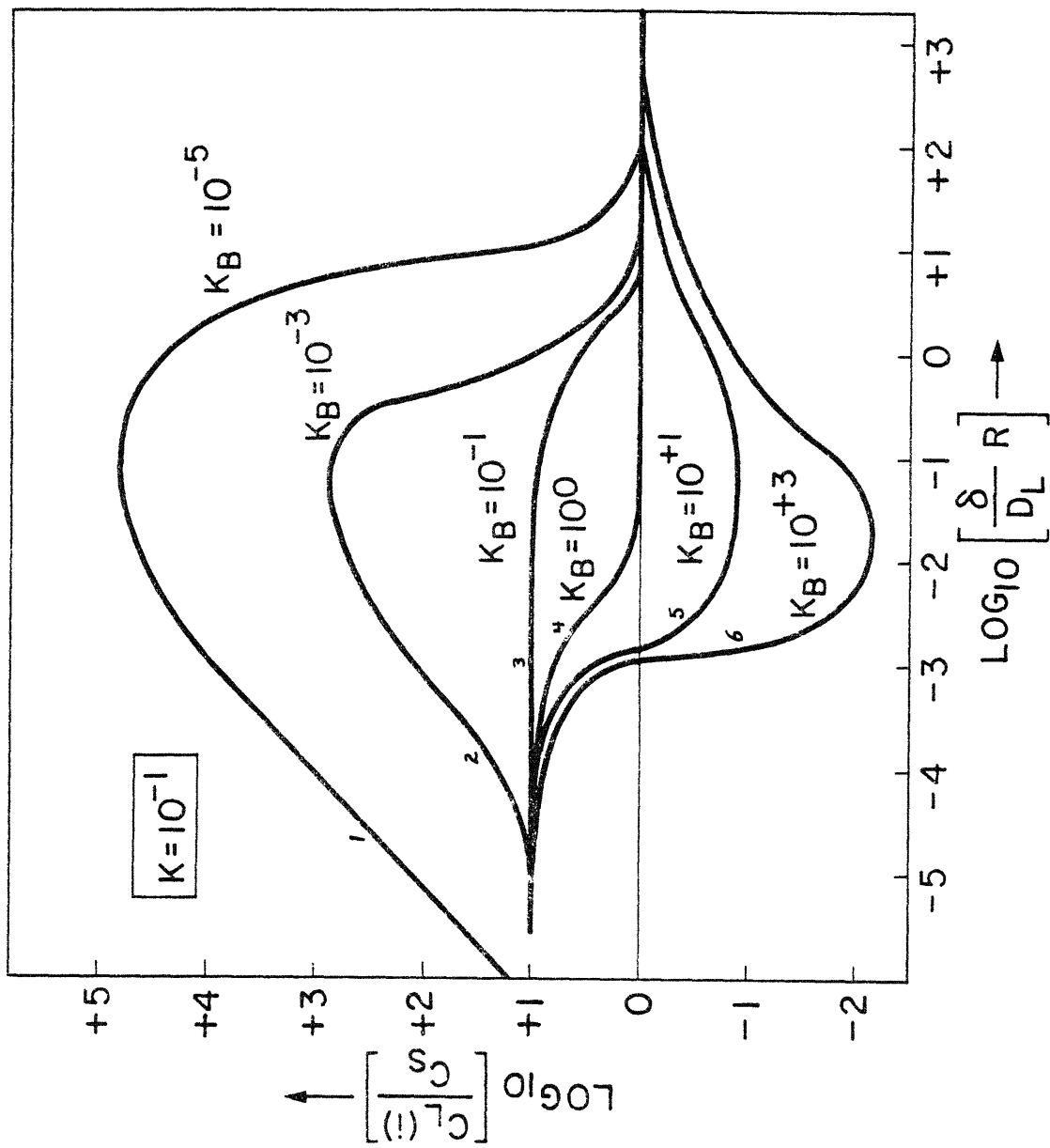


Figure V-2. Partitioning at interface as a function of imposed growth rate.

Chapter VI

SUMMARY AND GENERAL CONCLUSION

VI.1 Summary

We have seen that classical thermodynamics is useful and rigorous in determining free energy differences between various states of a system, thus indicating if certain changes of state are possible or not. Also thermodynamics is approximate but very useful when the condition of local equilibrium can be applied. But for the case of binary solidification it has been shown in Chapter II that the condition of local equilibrium at the interface does not always hold. And when the condition of local equilibrium at the interface is not valid for binary solidification, thermodynamics restricts the domain of the possible but it may still be so large that thermodynamics is inadequate in predicting what will happen.

The need to specify what will occur for situations similar to the above case has led to the development of the Theory of Irreversible Thermodynamics. The author has shown that this theory as currently applied is not rigorous or trustworthy, especially when applied to the interface processes during solidification. It predicts interface response functions which are of questionable validity. It is unreliable in attempts to restrict the liquid and solid interface compositions further than

classical thermodynamics has done as illustrated in Figure 1.7.

Due to the shortcomings in the ability of irreversible thermodynamics to predict correctly the interface response functions during solidification, the author has chosen an alternate method to the solution of the problem (Chapter V). By applying Solute Drag Theory, an expression has been found which relates the liquid and solid interface compositions to the imposed growth velocity. The analysis predicts solute trapping will always occur if the solute is surface active at the liquid-solid interface; otherwise it most likely will not occur.

The prediction of solute trapping during binary solidification is experimentally verified for Zn-Cd alloys in Chapter II.

VI.2 Suggestions for Future Work

The previous chapter concerned itself with deriving an expression for the interface partitioning during binary alloy solidification as a function of imposed steady-state velocity. But to describe "completely" the response of the interface in terms of the conditions at the interface another relationship involving the interface temperature T is needed. For a binary system two response functions are needed for a complete description. The author can think of a possible approach for determining this necessary

second relationship, but what may be first needed is additional experiments to study the deviations from local equilibrium, and to show whether or not there is interaction between various interface processes. An excellent experiment would be one which determines the exact direction of deviations in $C_L(i)$ and $C_S(i)$ in Figure 1.7 from their equilibrium values. Such an experiment would give much needed information on the nature of the interface processes; this would help in tightening restrictions for applying old principles or in developing new ones. Hence, better guidance would be available for formulating an expression for the second response function.

VI.3 References

1. K. A. Jackson, "Liquid Metals and Solidification," p. 174, Amer. Soc. for Metals, Cleveland (1958).
2. K. A. Jackson, Acta Met., 7, 148 (1959).
3. J. W. Cahn, Acta Met., 8, 554 (1960).
4. H. A. Wilson, Camb. Phil. Soc., 10, 25 (1898-1900).
5. F. C. Frank, Discussions of the Faraday Society, No. 5, p. 149 (1949); Phil. Mag., 41, 200 (1950).
6. W. B. Hillig and D. Turnbull, J. Chem. Phys., 24, 194 (1956).
7. D. Turnbull, Trans. AIME, 191, 661 (1951).
8. N. F. Mott, Proc. Phys. Soc., 60, 391 (1948).
9. K. T. Aust and J. W. Rutter, Trans. AIME, 215, 119 (1959), and *ibid.* 218, 682 (1960).
10. B. B. Rath and H. Hu, Trans. AIME, 245, 1577 (1969).
11. P. Gordon and R. A. Vandermeer, "Recrystallization, Grain Growth and Textures," p. 205, Amer. Soc. for Metals (1965).
12. K. A. Jackson and B. Chalmers, Can. J. Phys., 34, 473 (1956).
13. P. Niessen, Ph.D. Thesis, Univ. of Toronto (1964).
14. D. G. Cole, P. Feltham, and E. Gilliam, Proc. Phys. Soc., 67, 131 (1954).
15. P. Niessen and W. C. Winegard, J. Inst. Metals, 88, 300 (1963-64).
16. J. W. Gibbs, "On the Equilibrium of Heterogeneous Substances," Vol. 1, p. 219, Collected Works, Longmans, Green and Co., New York (1928).
17. J. W. Cahn, Acta Met., 10, 789 (1962).
18. L. S. Darken and R. W. Gurry, "Physical Chemistry of Metals," p. 215, Mc Graw-Hill Book Co., New York (1953).

19. Ref. 18; p. 240.
20. H. Biloni and B. Chalmers, Trans. AIME, 233, 373 (1965).
21. L. Kaufman and Morris Cohen, Prog. Metal Phys., Pergamon Press, 7, 165 (1958).
22. D. A. Karlyn, J. W. Cahn, and Morris Cohen, Trans. AIME, 245, 197 (1967).
23. K. A. Jackson, Can. J. Phys., 36, 683 (1958).
24. E. A. Owen and D. A. Davies, Brit. J. Appl. Phys., 16, 1291 (1965).
25. Pol Duwez and R. H. Willens, Trans. AIME, 227, 362 (1963).
26. V. T. Borisov, Soviet Phys.-Dok, 7, 50 (1962).
27. A. A. Chernov, "Growth of Crystals," Vol. 3, p. 35, Consultants Bureau, New York (1962).
28. J. R. Brown, J. Inst. Metals, 83, 49, 1954; R. W. Bohl and V. D. Hildebrandt, J. Am. Chem. Soc., 79, 2711 (1957).
29. C. D. Thurmond and J. D. Struthers, J. Phys. Chem., 57, 831 (1963).
30. Pol Duwez, Trans. ASM, 60, 607 (1967).
31. B. Chalmers, "Principles of Solidification," p. 129, John Wiley and Sons, New York (1964).
32. M. E. Glicksman and C. L. Vold, Acta Met., 15, 1409 (1967).
33. Ref. 31; p. 133.
34. W. W. Mullins and R. F. Sekerka, J. Appl. Phys., 35, 444 (1964).
35. S. R. de Groot and P. Mazur, "Non-Equilibrium Thermodynamics," North-Holland Publishing Co., Amsterdam (1962).
36. I. Prigogine, "Thermodynamics of Irreversible Processes," Interscience Publishers, New York and London (1961).
37. E. S. Machlin, Trans. AIME, 197, 437 (1953).

38. K. G. Denbigh, "The Thermodynamics of the Steady State," p. 29, John Wiley and Sons Inc., London (1958).
39. Ref. 36; p. 46.
40. L. Onsager, Phys. Rev., 37, 405 (1931); 38, 2265 (1931).
41. Ref. 35; p. 61-64.
42. B. D. Coleman and C. Truesdell, J. Chem. Phys., 33, 28 (1960).
43. G. Baralis, J. Cryst. Growth, 3-4, 627 (1968).
44. Ref. 36; p. 76.
45. J. S. Kirkaldy, Can. J. Phys., 37, 739 (1959).
46. J. W. Cahn and W. W. Mullins, "Decomposition of Austenite by Diffusional Processes," p. 123, Interscience Publishers, New York and London (1962).
47. Ref. 26.
48. I. L. Aptekar and D. S. Kamenetskaya, Fiz. Met. i. Metalloved, 14, 358 (1962).
49. B. K. Jindal and W. A. Tiller, J. Chem. Phys., 49, 4632 (1968).
50. V. T. Borisov, "Crystallization Processes," p. 69, Consultants Bureau, New York (1966).
51. W. T. Martin and E. Reissner, "Elementary Differential Equations," p. 60, Addison-Wesley Pub. Co. Inc., Reading, Mass. (1964).

VI.4 Biographical Note

The author, James C. Baker, was born in Flint, Michigan on May 24, 1942. He graduated from Flint Beecher High School in June, 1960. He entered Michigan State University in September, 1961 and graduated with a B.S. in Metallurgical Engineering in June, 1965. While an undergraduate he received membership to two engineering honoraries. He was the winner of a Wheelabrator Graduate Fellowship in 1965-66, and received his M.S. in Metallurgical Engineering at the University in June, 1966. During 1965-66 he also served as an instructor in the Metallurgy Department.

In September, 1966 the author entered M.I.T. as a Candidate for the Degree of Doctor of Philosophy in Materials Science. During his tenure he held a National Science Foundation Graduate Traineeship at the Institute.

Following the completion of his studies, the author will join the Homer Research Laboratories of Bethlehem Steel Corporation in Bethlehem, Pennsylvania.